Geophysical Journal International

Geophys. J. Int. (2018) **212,** 1932–1962
Advance Access publication 2017 November 24
GJI Geodynamics and tectonics

doi: 10.1093/gji/ggx509

Lithospheric structure along wide-angle seismic profile GEORIFT 2013 in Pripyat–Dnieper–Donets Basin (Belarus and Ukraine)

V. Starostenko,[1] T. Janik,[2] T. Yegorova,[1] W. Czuba,[2] P. Środa,[2] D. Lysynchuk,[1] R. Aizberg,[3] R. Garetsky,[3] G. Karataev,[3] Y. Gribik,[3] L. Farfuliak,[1] K. Kolomiyets,[1] V. Omelchenko,[1] K. Komminaho,[4] T. Tiira,[4] D. Gryn,[1] A. Guterch,[2] O. Legostaeva,[1] H. Thybo[5,6,7] and A. Tolkunov[8]

[1]*Institute of Geophysics, National Academy of Sciences of Ukraine, UA*-03142 *Kiev, Ukraine. E-mail: myronivska@gmail.com*
[2]*Institute of Geophysics, Polish Academy of Sciences, PL*-01-452 *Warsaw, Poland*
[3]*Institute for Nature Management, National Academy of Sciences of Belarus,* 220114 *Minsk, Belarus*
[4]*Department of Geosciences and Geography, Institute of Seismology, University of Helsinki, FI*-00014 *Helsinki, Finland*
[5]*Department of Geography and Geology, University of Copenhagen, DK*-1350 *Copenhagen, Denmark*
[6]*Eurasia Institute of Earth Sciences, Istanbul Technical University,* 34469 *Istanbul, Turkey*
[7]*Centre for Earth Evolution and Dynamics, University of Oslo, NO*-0371 *Oslo, Norway*
[8]*State Geophysical Enterprise "Ukrgeofizika", UA*-03057 *Kiev, Ukraine*

Accepted 2017 November 23. Received 2017 November 22; in original form 2017 July 20

SUMMARY

The GEORIFT 2013 (GR'13) WARR (wide-angle reflection and refraction) experiment was carried out in 2013 in the territory of Belarus and Ukraine with broad international co-operation. The aim of the work is to study basin architecture and deep structure of the Pripyat–Dnieper–Donets Basin (PDDB), which is the deepest and best studied Palaeozoic rift basin in Europe. The PDDB is located in the southern part of the East European Craton (EEC) and crosses Sarmatia—one of the three segments of the EEC. The PDDB was formed by Late Devonian rifting associated with domal basement uplift and magmatism.

The GR'13 extends in NW–SE direction along the PDDB strike and crosses the Pripyat Trough (PT) and Dnieper Graben (DG) separated by the Bragin Uplift (BU) of the basement. The field acquisition along the GR'13 (of 670 km total length) involved 14 shots and recorders deployed every ∼2.2 km for several shot points. The good quality of the data, with first arrivals visible up to 670 km for several shot points, allowed for construction of a velocity model extending to 80 km depth using ray-tracing modelling. The thickness of the sediments (Vp $<$ 6.0 km s^{-1}) varies from 1–4 km in the PT, to ∼5 km in the NW part of the DG, to 10–13 km in the SE part of the profile. Below the DG, at ∼330–530 km distance, we observed an upwarping of the lower crust (with Vp of ∼7.1 km s^{-1}) to ∼25 km depth that represents a rift pillow or mantle underplate. The Moho shallows southeastwards from ∼47 km in the PT to 40–38 km in the DG with mantle velocities of 8.35 and ∼8.25 km s^{-1} in the PT and DG, respectively. A near-horizontal mantle discontinuity was found beneath BU (a transition zone from the PT to the DG) at the depth of 50–47 km. It dips to the depth of ∼60 km at distances of 360–405 km, similar to the intersecting EUROBRIDGE'97 profile.

The crust and upper mantle structure on the GR'13 may reflect varying intensity of rifting in the PDDB from a passive stage in the PT to active rifting in the DG. The absence of Moho uplift and relatively thick crystalline crust under the PT is explained by its tectonic position as a closing unit of the PDDB, with a gradual attenuation of rifting from the southeast to the northwest. The most active stage of rifting is evidenced in the DG by a shallower Moho and by

a presence of a rift pillow caused by mafic and ultramafic intrusions during the active phase. The junction of the PT and the DG (the BU) locates just at its intersection with the NS regional tectonic zone Odessa-Gomel. Most likely, the 'blocking' effect of this zone did not allow for further propagation of active rifting to the NW.

Key words: Europe; Controlled source seismology; Wave propagation; Continental tectonics: extensional; Crustal structure; Intra-plate processes.

1 INTRODUCTION

The East European Craton (EEC) is an ancient stable core of the European continent. It consists of an ensemble of continental plates and microplates that were welded together in the Late Proterozoic (Bogdanova 1993; Bogdanova *et al.* 1996). One of the key processes of the Phanerozoic history of the EEC was the Late Palaeozoic rifting occurring almost throughout the EEC (Nikishin *et al.* 1996; Stephenson *et al.* 2006). Most strongly these processes appeared as intracratonic rifting in the Pripyat–Dnieper–Donets Basin (PDDB) on the southern margin of the EEC. PDDB is a rift system that is composed of three basins of approximately equal area and differing tectonic development. Furthermore a rift system is an area where the lithosphere is thinning, typically associated with large faults and grabens. Therefore, the study of continental rifting on the example of the PDDB, with its well preserved structural and stratigraphic record, seems to be very important target for the present seismic survey on the GEORIFT 2013 (GR'13) profile (Figs 1 and 2).

The sedimentary cover of the EEC is one of the best natural laboratories to study tectonic processes and intraplate deformations related with processes occurring at the plate boundaries and in the mantle. The extended PDDB was formed in the SE part of the EEC as a result of Late Devonian rifting in the arch of ancient Sarmatian Shield (Khain 1977), forming a large basement uplift with a diameter of about 1000 km (Stephenson *et al.* 1993). The main segments of the PDDB rift system—non-inverted Pripyat Trough (PT) and Dnieper Graben (DG) and inverted Donbas Foldbelt (DF)—control the location of large coal- and hydrocarbon-bearing as well as saliferous industrial provinces in Belarus and Ukraine.

The GR'13 was an international collaborative project with participation of institutions from Ukraine, Belarus, Poland, Finland and Denmark. Seismic data acquisition was undertaken in August 2013. The NW–SE transect of 670 km total length extended along the PT and the DG of the PDDB, which are the deepest and best studied Palaeozoic rift basins in Europe.

Geological investigations in the area of the PDDB have begun since the end of 19 century (Karpinsky 1883, Chirvinsky 1928). The 1960s–1980s of the last century are marked by rapid growth of geophysical research in the former Soviet Union, and, in particular, in the PDDB region. During that period the DG was covered with a network of the DSS (deep seismic sounding) profiles including 13 lines crossing the rift zone, spaced at a distance of 50–150 km from each other, and one extended profile along the rift zone axis (Sollogub 1980, 1986). Selected DSS lines are shown in Figs 1 and 2. Interpretation of these materials made it possible to reveal the general features in the structure of the crust of the rift zone, such as variations in thickness of the sedimentary cover and of the crust along and across the rift zone, to study the relief of the Moho, and also to locate a high-velocity body in the lower-middle crust below the graben. At this time, deep seismic reflection studies were carried out on two profiles crossing the PT (one of them, the profile VIII, is shown in Figs 1 and 2), which made it possible to image the basement and discontinuities in the crust and upper mantle (Garetsky & Klushin 1989).

Since the 1990s of the last century, numerous modern WARR studies, sometimes together with deep reflection studies (CDP), were conducted in the framework of international projects involving participants from many countries. In 1996 and 1997, the PT was crossed by two WARR profiles—the EUROBRIDGE'96 and EUROBRIDGE'97 (EUROBRIDGE Seismic Working Group 1999; Thybo *et al.* 2003). The DF was the target for seismic investigations acquired in 1999–2000 on the DOBRE'99 profile including the WARR and CDP surveys (DOBREfraction'99 Working Group 2003; Maystrenko *et al.* 2003). At that time, some of the previous seismic lines were reinterpreted using modern techniques—CDP profile VIII (Juhlin *et al.* 1996), DSS profile Piryatin-Talalevka (Baranova & Kozlenko 1989; Ilchenko *et al.* 1996) and DSS lines Kiev-Gomel and Yagotin-Baturin (Baranova & Kozlenko 1989).

A large number of geological and geophysical studies (deep drilling, seismic profiling, etc.) were carried out in this region (Garetsky 1979; Chirvinskaya & Sollogub 1980; Eisenverg 1988; Gavrish 1989; Ulmischek *et al.* 1994). The PDDB was also the key region of one of the projects of the EUROPROBE program (Gee & Zeyen 1996). The results obtained have been published in a series of special issues of the *Tectonophysics* (Stephenson *et al.* 1996, 1999; Stephenson 2004) and in the papers Bogdanova & Garetsky (2006), Bogdanova *et al.* (2006), Starostenko & Stephenson (2006) and Stephenson *et al.* (2006).

Most of the previous investigations were carried out along the profiles crossing the rift zone at high angles (Figs 1 and 2). Moreover, they were focused mainly on reflected phases, which provided only little information on seismic velocities. The GR'13 experiment, thanks to the usage of modern seismic stations, allowed us to obtain traveltime curves of reflected and refracted waves at offsets significantly larger than for past experiments, and to produce a more detailed velocity model of the crust and upper mantle. The GR'13 results, together with previous information, will allow us to study the PDDB as a whole, as well as to investigate the crustal structure of its individual segments, and to understand better the processes of Late Palaeozoic intracratonic rifting and the evolution of the rift system on the southern margin of the EEC.

2 REGIONAL GEOLOGICAL AND GEOPHYSICAL BACKGROUND

2.1 Geological and tectonic background

The PDDB was formed on the southeastern margin of the EEC as a result of Late Devonian rifting in the arch of the ancient Sarmatian Shield (Khain 1977) or Sarmatia (Bogdanova *et al.* 1996). Sarmatia, the southernmost of three major segments forming the EEC, includes the Archean-Palaeoproterozoic Ukrainian Shield (UkS) and the Voronezh Massif (VM), which are separated from each other

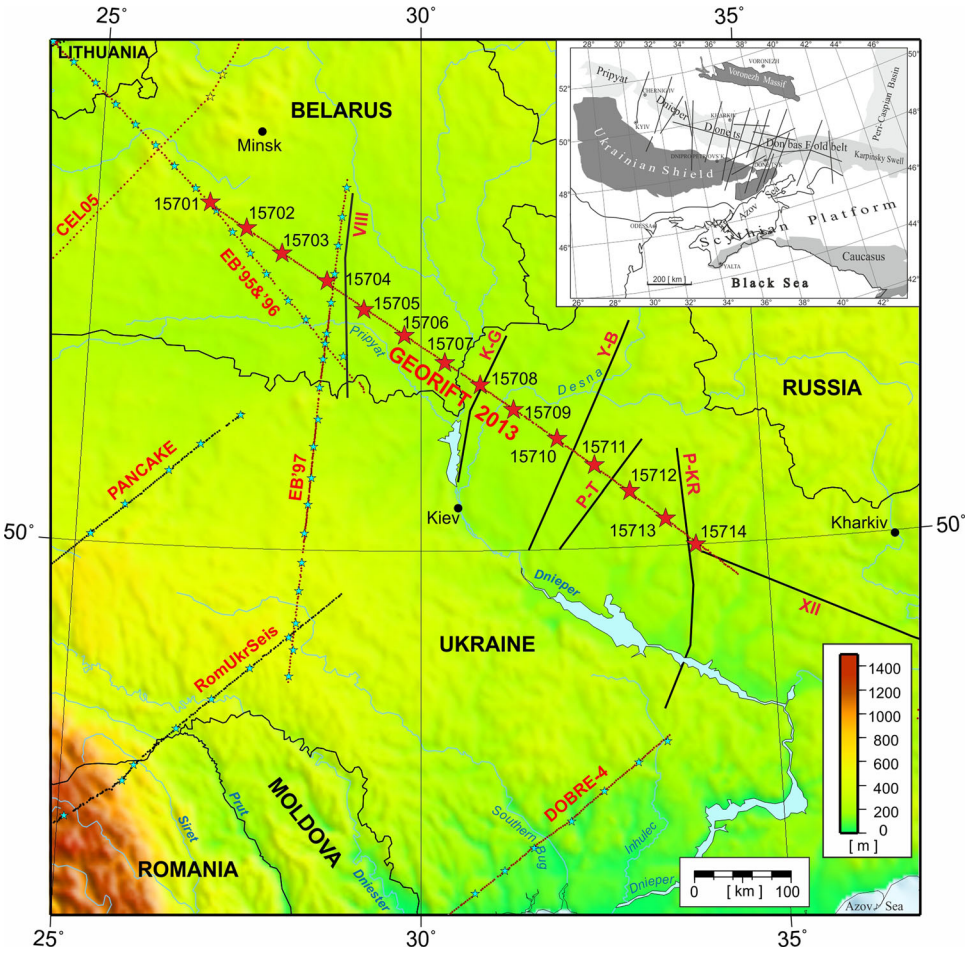

Figure 1. Location of the composite GEORIFT 2013 profile and previous refraction seismic profiles in the study area. Stars represent shot points; dots represent recording stations. Abbreviations of profiles: K-G, Kiev–Gomel; Y-B, Yagotyn–Baturin; P-T, Piryatyn–Talalaivka; P-KR, Putyvl-Krivoi Rog; XII, geotraverse XII (Poltava–Sverdlovsk); VIII, deep CDP line—all these lines represent main parts of the profiles. More lines are shown on the inset map showing the location of the Pripyat–Dnieper–Donets Basin and adjacent tectonic units at the southern part of the East European Craton.

by the PDDB intracratonic rift. Crystalline basement is exposed in the UkS and VM. The VM and, especially, the UkS have traditionally been divided into regional 'blocks' or lithotectonic basement complexes separated by nearly N–S-oriented sutures or 'interblock zones' of Proterozoic age. Several of these can be correlated across the PDDB (Fig. 2; Shchipansky & Bogdanova 1996). According to this, the GR'13 profile crosses from NW to the SE the following crustal domains (Fig. 2): the Osnitsk-Mikashevichi Igneous Belt (OMIB) of ~2.0–1.95 Ga age (overlain by the PT), the Bryansk Block (corresponding to the Bragin Uplift, BU)—a part of the large Bryansk-Bragin granulite domain, formed between *ca.* 2.2 and 2.1 Ga ago, and the Sevsk-Ingul crustal domain (2.2–2.1 Ga), containing Archean rocks of *ca.* 3.1–2.8 Ga age.

The tectonic position of NE–SW trending OMIB is still under discussion. The OMIB is considered by Aksamentova (2002) as a magmatic province formed during 2.1–1.7 Ga and associated with the development of the middle-Palaeoproterozoic deep faults of SE strike. According to Bogdanova *et al.* (2006), the OMIB is a suture zone with traces of Andean-type magmatism, separating Sarmatia and Fennoscandia; the latter includes the Central Belarus zone (Fig. 2).

The Bryansk-Bragin granulite domain, underlying the SE end of the PT and the NW part of the DG, is exposed at the BU that separates the PT and the DG (Fig. 2). The rocks composing the domain are attributed by Aksamentova & Naidenkov (1990) to the Archaean, whereas Bogdanova *et al.* (2006) consider them as analogues and continuation of the Teterev series of the Ukrainian Shield of Palaeoproterozoic age.

The rift system includes non-inverted segments of the PT and the DG, as well as inverted DF segment. The PT is an asymmetric sedimentary basin of about 280 km length, up to 150 km width and with sedimentary thickness of 2–6 km. It is separated from the DG by the BU of the basement, where the rift zone narrows and changes its general strike, and associates with the maximum intensity of Late Devonian volcanism (Garetsky 1979; Chirvinskaya & Sollogub 1980; Lyashkevich & Marushkin 1982; Lyashkevich 1987). The width of the DG varies from 60–70 km in the northwest to 140–160 km in the southeast. Similarly, the maximum thickness of sediments increases southeastwards from 4 to 22 km (Sollogub *et al.* 1977; Chekunov *et al.* 1993; Kivshik *et al.* 1993). Rifting was accompanied by intense magmatic activity in the late Devonian (Lyashkevich 1987; Wilson & Lyashkevich 1996).

It is believed that the rift system of the PDDB is located within the longer tectonic zone of the Sarmato-Turanian lineament, which extends in NW–SE direction from Poland to the Caspian Sea (Aizberg *et al.* 1971). The PDDB could be related with the formation of the Peri-Caspian basin as a system of Late Devonian rift zones at

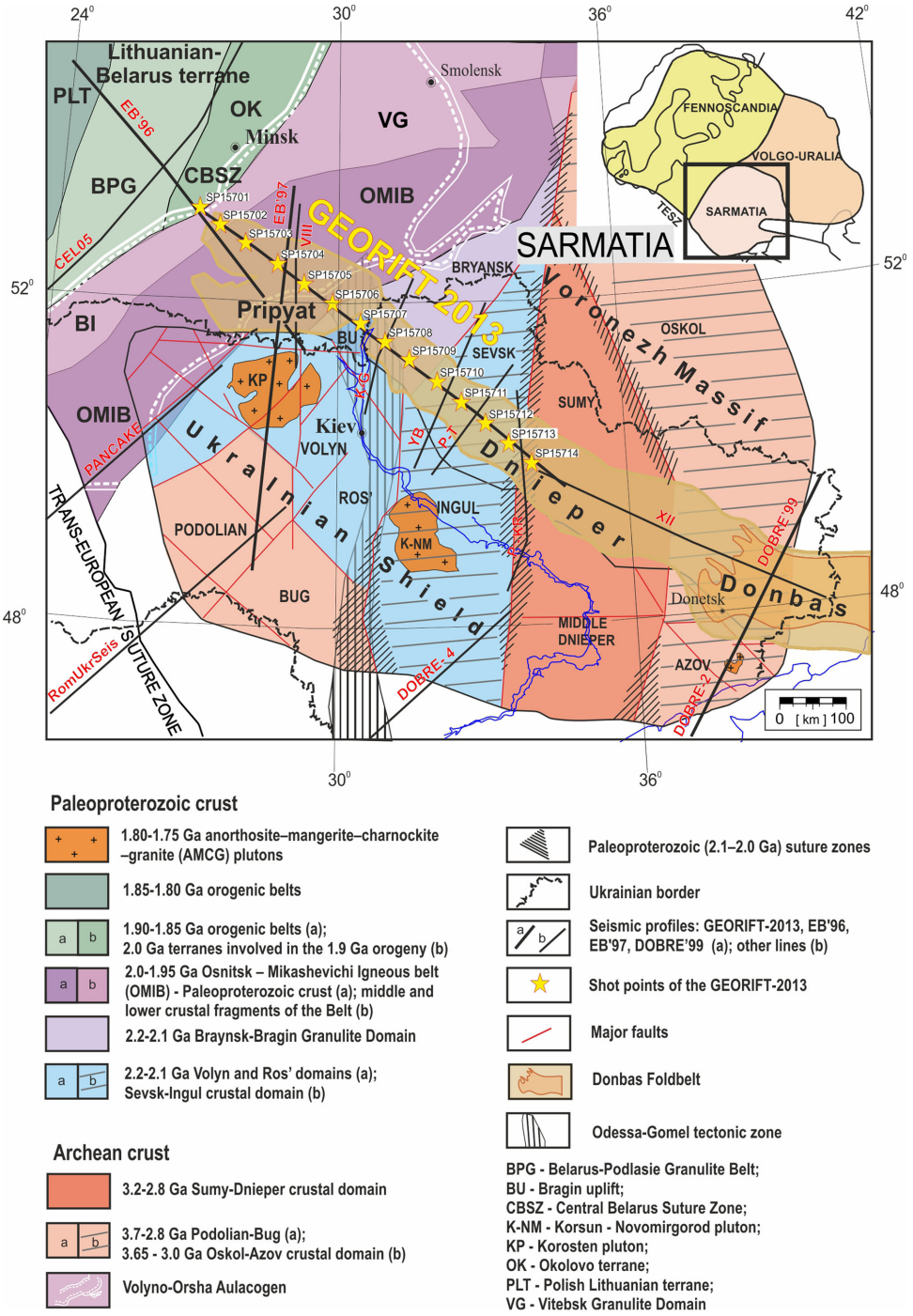

Figure 2. Tectonic map of the Pripyat–Dnieper–Donets Basin (PDDB) and location of the GEORIFT 2013 WARR profile. The PDDB is located in the southeastern part of Sarmatia (Bogdanova *et al.* 1996) that includes the Archean-Paleoproterozoic Ukrainian Shield (UkS) and the Voronezh Massif (VM), which are separated by the PDDB. The UkS and VM are traditionally mapped in terms of lithotectonic basement complexes (domains) separated by nearly N–S oriented sutures or 'interblock zones' of Proterozoic age. Several of these can be correlated across the PDDB from the UkS to the VM (Shchipansky & Bogdanova 1996). According to this, the GEORIFT 2013 crosses the following Palaeoproterozoic crustal domains: the Osnitsk-Mikashevichi Igneous Belt (OMIB) overlain by the Pripyat Trough, the Bryansk Block (corresponding to Bragin Uplift) that is the part of large Bryansk-Bragin granulite domain and Sevsk-Ingul crustal domain that contains Archean rocks. The southeastern end of profile is located at the Archean block Sumy—Middle Dnieper.

the southern margin of the EEC (Zonenshain *et al.* 1990; Chekunov 1994; Wilson & Lyashkevich 1996; Yegorova *et al.* 2004a; Stephenson *et al.* 2006).

The Late Devonian rifting and associated domal basement uplift and magmatism were widespread in the EEC (Wilson & Lyashkevich 1996; Stephenson *et al.* 2006). Most probably, magmatism was triggered by the upwelling of a thermally and geochemically anomalous magma from the base of the lithosphere. The peak of magmatic activity occurred in the Famennian (Wilson & Lyashkevich 1996). The DG is characterized by the main extension occurring between the late Frasnian (370 Ma) and the end of Devonian (363 Ma), linear bounding crustal faults, significant crustal

thinning ($\beta \sim 1.3$) and abundant syn-rift volcanic activity (Kusznir *et al.* 1996a). In the PT, characterized by much smaller amounts of extension ($\beta \sim 1.1$–1.13), the major part of rifting occurred extremely rapidly between 367 and 364 Ma, with little associated magmatic activity (Kusznir *et al.* 1996b).

The geochemical signature of rift-related magma (Wilson & Lyashkevich 1996) and its sheer volume suggest that the origin of the rift zone is mantle plume/hotspot related (e.g. Gavrish 1989; Chekunov 1994; Wilson & Lyashkevich 1996; Kusznir *et al.* 1996a; *cf.* Stephenson *et al.* 2006). Subsidence modelling studies suggest that thinning of the mantle lithosphere was greater than crustal thinning (e.g. van Wees *et al.* 1996; Starostenko *et al.* 1999; Poplavskii *et al.* 2001). This could be an evidence for active rifting involving thermal processes in the mantle (Saintot *et al.* 2006; Stephenson *et al.* 2006). This Late Devonian rifting is not manifested in the present day heat flow observed in the surface, which is characterized by almost constant level with 45 mW m^{-2} value (Kutas & Gordienko 1971). Local anomalies of the heat flow relate to salt diapirs and fluid flows.

The magmatic activity, represented by alkaline-ultramafic lavas, alkali basalts and their differentiates, occurred along major syn-rift faults and at their intersections with older basement faults. Most likely, only a small amount of magma was erupted, the rest being emplaced within the crust as sills/dykes and as an extensive mafic crustal underplate (Wilson 1993; Wilson & Lyashkevich 1996). The latter can be seen in many of the DSS lines across the rift as a high-velocity/density layer in the mid-lower crust (Stephenson *et al.* 1993; Ilchenko 1996; DOBREfraction'99 Working Group 2003) evidenced by associated magnetic and gravity anomalies along the axis of the DG (Starostenko *et al.* 1986; Yegorova *et al.* 1999, 2004a).

The distinctive feature of the PDDB is the occurrence of major salt deposits in the syn-rift sequence. Extensive remobilization of this salt horizon during the Late Devonian—Early Permian led to formation of numerous salt diapirs, particularly in the PT (Fig. 3; Garetsky 1979; Ulmishek *et al.* 1994). The salt diapirs locally exhumed fragments of mafic igneous rocks from deeper levels of the basin. The Frasnian–Famennian succession contains interbedded clastic and carbonate sediments, salt and volcanic and volcaniclastic rocks (Kusznir *et al.* 1996a,b).

A Permian unconformity is evident throughout the southern part of the PDDB, where the Early Permian uplift affecting the southern margins of the DG and the DF occurred in a transtensional tectonic regime (Stephenson *et al.* 2001). Basin inversion in the DF occurred mainly in the Late Cretaceous due to compression caused by Alpine deformations.

2.2 Reflection seismic studies and structure of the sedimentary cover along the GR'13 profile

Results of deep seismic reflection studies along two profiles crossing the PT (one of them (VIII) is shown in Figs 1 and 2; Garetsky & Klushin 1989) and on the DOBRE'99 profile in the DF (Maystrenko *et al.* 2003) revealed reflections from the basement, from the boundaries in the crust and upper mantle. In the border zones of the PT, a large number of inclined reflectors associated with listric faults were observed. Reinterpretation of these data made by Juhlin *et al.* (1996) has shown numerous steeply dipping listric faults extending from the surface to the top of reflective lower crust (at 30–40 km depth), with the Moho at 45–50 km.

Deep seismic reflection studies were not carried out in the DG. A total of 19 oil and gas exploration CDP lines have been acquired in the DG across the rift zone with the profile length increasing from ~ 100 km to the NW to 160 km to SE, and a series of profiles along the northern and southern flank zones were also made (Kivshik *et al.* 1993; Stovba *et al.* 1995, 1996; Stovba & Stephenson 1999). With the increase in the depth of the basement, registration time was increased to >8 s.

Descriptions of regional architecture of the PDDB and sedimentary succession are given in many papers (Garetsky 1979; Chirvinskaya & Sollogub 1980; Eisenverg 1988; Garetsky & Klushin 1989; Chekunov *et al.* 1992a; Stephenson *et al.* 1993; Chekunov 1994 Ulmishek *et al.* 1994; Juhlin *et al.* 1996; Stovba *et al.* 1996; Stovba & Stephenson 1999). ***Pre-rift succession*** corresponds to pre-late Frasnian ($D_{2\text{-}3}$) sediments (Fig. 3) and comprises the so-called 'undersalt' strata composed of sandstones, siltstones, clays and carbonates. ***Syn-rift succession*** is composed of Late Frasnian–Famennian (D_3) salt ('lower' and 'upper' salt) alternated with clastic and carbonates. The syn-rift succession is accompanied by intense volcanism, tectonic movements along the border faults, development of grabens and half-grabens. ***The post-rift*** successions are well developed in the DG, but poorly visible in the PT. They are composed of Carboniferous and younger sediments with thickness increases southeastwards from 1 km in the PT to 11 km in the DG.

Geological cross-section of the sedimentary cover on the GR'13 profile (Fig. 3) was constructed along the PT and the DG using data from 40 wells, located at ~1.9 km of average distance from the profile, and reflection seismic profiling data (Pobedash 2015).

In general, the PT is filled with sedimentary deposits of the Lower Devonian–Middle Triassic. Devonian sediments, having maximum thickness of deposits in the whole section, contain two above-mentioned halite strata of the Frasnian and Famennian age ('lower' and 'upper' salt layers) (Fig. 3; Garetsky 1979; Ulmishek *et al.* 1994). In the PT the GR'13 profile crosses from the NW to the SE the Chervonosloboda-Malodushin and the Azeretsk-Khobninsk Thresholds, the Axial Graben and the BU, where thickness of sediments increases from 1.5–2.0 km in the westernmost part to 4 km in the Axial Graben, and then thins again to ~1 km at the BU (Fig. 3). All the main units are separated by faults.

Intense salt tectonics occurred in the Azeretsk-Khobninsk Threshold with formation of numerous salt domes and diapirs in the upper salt layer with a salt thickness up to 2 km (Fig. 3). On the Khoinik Uplift the thickness of the halite strata dramatically reduces. On the BU the crystalline basement is covered by thin terrigenous and carbonate undersalt strata and a thin salt layer.

In the DG, the GR'13 profile passes through a series of depressions and troughs separated by projections and uplifts of the basement, which are limited by faults of amplitude varying from 100 to 800 m. Devonian and younger sediments thicken in the southeastern direction. In the western part of the DG, the profile passes through the Skorynetska depression, and a broad, elongated along the GR'13 profile, Nizhyn trough filled with sediments as thick as 5.5–6.0 km (Fig. 3). The latter is separated by several basement highs from wide Sribnenska depression with thickness of sediments up to 8.5 km. In the area of one of them—the Augustovsky high, a series of salt stocks is observed (one of them is shown in Fig. 3). Further southeastwards, the Sribnenska depression passes into the North-Yarov Trough, which is separated by the Sulimov Uplift from the Landaryiska depression—the last and the deepest one (12 km depth) on the GR'13 profile (Fig. 3).

The sedimentary cover along the GR'13 profile is represented by almost all stratigraphic complexes determined in the PDDB—from quite thick pre-rift and syn-rift Devonian sediments to thinner post-rift sediments of Carboniferous and Mesozoic age.

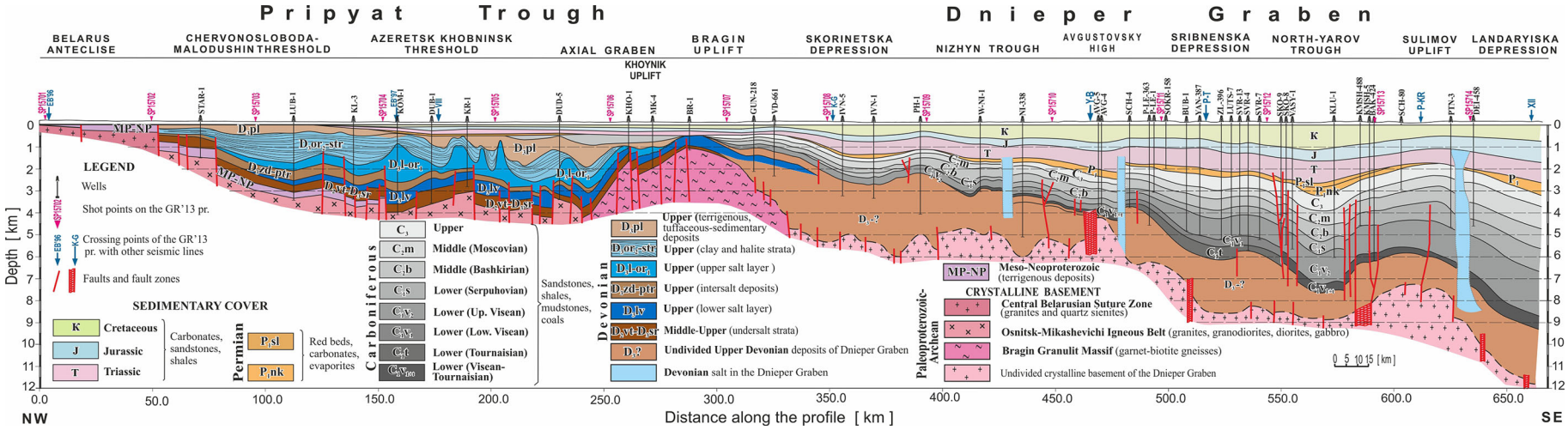

Figure 3. Geological cross-section along the GR'13 profile through the Pripyat Trough (PT) and Dnieper Graben (DG) based on reflection seismics and borehole data from (Pobedash 2015). Vertical exaggeration is 10:1. Boreholes in the PT: BR-1, Bragin-1 (3 km to N); DUB-1, Dubnyak-1 (1 km to N); DUD-5, Dudich-5 (1 km to S); KHO-1, Khoynik-1 (3.3 km to S); KL-3, Kalinov-3 (0.5 km to S); KOM-1, Komarovych-1 (4.0 km to N); KR-1, Krotov-1 (2.5 km to S); LUB-1, Liubun-1 (4.7 km to N); MK-4, Mykulich-4 (4.5 km to S); STAR-1, Starobyn-1 (14 km to S). Boreholes in the DG: AVG-4, Avgustiv-4 (0.5 km to S); AVG-5, Avgustiv-5 (1.5 km to S); BAK-424, Bakumiv-424 (0.5 km to S); BUB-1, Bubchenkiv-1 (1 km to S); DEI-458, Deinekiv-458 (0.5 km to S); GUN-218, Gunkiv-218 (3.5 km to S); IVN-1, Ivanytsk-1 (1.5 km to N); IVN-5, Ivanytsk-5 (1.5 km to N); KLU-1, Klushnykiv-1 (0.5 km to S); KMSH-488, Komyshnyansk-488 (1.5 km to S); KMSH-5, Komyshnyansk-5 (0.5 km to S); LUTS-7; Lutsenkiv-7 (2 km to S); NI-338, Nigzyn-338 (5 km to S); PH-1, Perehodiv-1 (on the line); P-LE-1, Perevolochansk-Lelyakiv-1 (4.5 km to S); P-LE-363, Perevolochansk-Lelyakiv-363 (1 km to S); PTN-3, Petrenkiv-3 (on the line); SCH-4, Schuriv-4 (on the line); SCH-80, Sorochyn-80 (2 km to N); SKO-8, Skorobagatkiv-8, (3 km to N); SKO-9; Skorobagatkiv-8, (1 km to N); SOKR-158; Sokyryntsi-158 (on the line); SVR-13, Svyrydiv-13 (on the line); SVR-4, Svyrydiv-4 (1 km to N); SVR-7, Svyrydiv-7 (2 km to N); VASY-1, Vasylky-1 (on the line); VD-661, Videltsiv-661 (0.5 km to S); W-NI-1, West-Nizgyn (0.5 km to S); YAN-387, Yabluniv-387 (on the line); ZL-396, Zasulsk-396 (on the line).

Table 1. Location and parameters of shot points for profile GEORIFT 2013.

Shot point number	Distance (km)	Latitude N (φ)	Longitude E (λ)	Altitude h (m)	Time UTC (y:d:h:m:s)	TNT charge (kg)
SP15701	3.179	53.20519	26.73396	198	2013:227:20:59:52.53	1000
SP15702	48.740	52.97725	27.30867	183	2013:229:21:00:12.60	800
SP15703	93.689	52.75626	27.86751	144	2013:231:21:00:09.09	800
SP15704	148.601	52.50451	28.56549	118	2013:231:21:30:10.23	700
SP15705	197.079	52.24444	29.13819	137	2013:229:21:59:33.31	700
SP15706	246.832	52.00736	29.75458	128	2013:227:22:00:01.86	600
SP15707	297.099	51.75444	30.35944	117	2013:227:23:00:19.99	600
SP15708	340.491	51.54100	30.88431	144	2013:227:22:30:55.29	600
SP15709	383.570	51.30769	31.37914	120	2013:228:20:59:46.75	600
SP15710	437.361	51.02900	32.00761	131	2013:227:23:31:26.11	700
SP15711	484.675	50.77528	32.54750	128	2013:228:21:31:24.71	700
SP15712	530.296	50.52289	33.05619	127	2013:229:21:31:23.56	800
SP15713	576.779	50.25110	33.55422	118	2013:228:22:01:52.00	800
SP15714	617.937	50.00015	33.97996	95	2013:227:21:31:36.15	1000

The thickness of the latter considerably increases in the southeastern direction.

2.3 Previous deep seismic refraction studies

In the 1960s–1970s of last century, the Dnieper–Donets basin was covered with a network of the DSS profiles. Most of them crossed the rift zone, and one extended along the rift axis (Sollogub 1980, 1986; Figs 1 and 2). The observed wave field is represented by refracted and near-vertical reflected waves. The *P*-waves were recorded at the offsets of up to 250 km, the average length of the traveltime curves was about 150 km.

Interpretation of the wave field revealed the general features of the subsurface and deep structure of the rift zone and adjoining parts of the Ukrainian Shield and the Voronezh Massif (Sollogub 1986; Baranova & Kozlenko 1989; Pavlenkova 1995; Ilchenko 1996). It has been shown that thickness of the crust and inner crustal structure change considerably across and along the rift basin. Below the central part of the DG, the Moho rises a few kilometres relative to the flank zones. The thickness of the crystalline crust decreases southeastwards from 30–35 km to 20–25 km due to thickening of sediments in the graben. A distinctive feature of the rift zone, seen on most DSS profiles and most clearly manifested in the Piryatin-Talalaevka profile (Ilchenko 1996), is the occurrence of higher crustal velocities beneath the rift than beneath flanking areas. In the Donets segment, a crust–mantle transition zone with velocities of about 7.6 km s^{-1} overlies upper mantle (8.0 km s^{-1}). It should be noted, however, as clearly demonstrated by Ilchenko (1996), that velocities beneath the upper crust, including those of the high velocity "crust–mantle" lens, are poorly constrained (being not controlled by refracted seismic phases) in all of the earlier data sets.

The PT is crossed by two recent WARR profiles—the EUROBRIDGE'96 and EUROBRIDGE'97 (EUROBRIDGE Seismic Working Group 1999; Thybo *et al.* 2003), which shows the crystalline crust thickness of ~45 km, with thin upper crust and thick middle crust with Vp = 6.4–6.75 km s^{-1}. The distinctive feature of the uppermost mantle below the PT on the EUROBRIDGE'97 is a major reflector that dips in SSW direction below the Ukrainian Shield. It extends from the Moho down to the depth of c. 75 km (Thybo *et al.* 2003).

The DF, which is the southeastern inverted part of the PDDB, is crossed by the DOBRE'99 profile, along which the WARR and deep CDP studies were carried out (DOBREfraction'99 Working Group 2003; Maystrenko *et al.* 2003). These studies show a well-defined sedimentary basin, overlying main crustal layer with a high-velocity lower crustal layer that thickens significantly beneath the main sedimentary depocentre.

2.4 Gravity and magnetic field of the PDDB area

The segmentation of the PDDB is reflected by the patterns of geophysical fields. The gravity low of the PT of −55 mGal amplitude turns into intense Chernigov maximum of >90 mGal centred at the BU, which is among the highest of the whole EEC. This maximum coincides with the occurrence of significant volumes of Late Devonian, rift-related, volcanics and intrusive rocks. The Chernigov maximum is an extreme western anomaly in a series of axial gravity highs of the DG (Chirvinskaya & Sollogub 1980). Further southeastwards, their amplitudes decrease from 50 to 30 mGal at the southeastern end of the profile, in accordance with the thickening of sediments from 4 to >10 km. These positive gravity anomalies along the rift axis are considered to be caused by the intrusion of mafic/ultramafic mantle rocks into the lower crust during rifting (Starostenko *et al.* 1986; Yegorova *et al.* 1999, 2004a; Kozlovskaya *et al.* 2004).

The magnetic field also shows the segmentation of the PDDB depending on the depth and composition of the basement. The magnetic field pattern of the PT is represented by intense mosaic-like anomalies with amplitude up to 800–1000 nT that constitute a belt of magnetic anomalies of general NE strike above the OMIB with the bodies of diorite and intrusions of gabbro (Aksamentova 2002). In the NW part of the DG, with thickness of sediments <4–5 km, there are two large magnetic highs, elongated along the rift strike, more intense in the area of Chernigov (400–500 nT) and another one of lower intensity, but wider, in the region of Poltava (Pashkevich *et al.* 2014). Both highs coincide with the gravity anomalies and are caused by Devonian effusive rocks in the sedimentary cover and, probably, by intrusive rocks in the basement and upper crystalline crust.

3 DATA ACQUISITION AND PROCESSING

GR'13 transect is placed on the territory of Belarus and Ukraine in near equal parts. The total profile length is 670 km: 315 km on the Belarusian territory and 360 km in Ukraine. The field acquisition involved 14 shot points (charge 600–1000 kg of TNT) every ~35–50 km (seven shot points in Belarus and seven in Ukraine), and 309 recording stations placed every ~2.2 km.

Details of the seismic sources are given in Table 1. As sources, explosives distributed in an array of drilled holes, with total shot

sizes varying between 600 and 1000 kg, were used. Every shot point consisted of wells group with the charge of 50 kg per well. The depth of the wells was close to 20 m. largest shots were located close to profile ends and smallest shots were placed in the central part. The recording geometry of large shots was designed to obtain long branches of the P_n arrivals (refractions from the uppermost mantle). The smaller shots provided necessary ray coverage of the crust. However, good transmission properties of rocks also allowed us to correlate different reflections and refractions, including P_n, for smaller shots as well. All shots in Belarus territory were drilled and fired by Central Geophysical Expedition. Ukrainian shots were fired by state enterprise 'KRYMVYBUKHPROM', but drill holes were prepared by 'UKRGEOFIZIKA'.

After field acquisition and initial data processing, 150 s long seismograms starting at each shot time were extracted. The extracted traces and geometry information were collated into a common data set of shot gathers. For several shot points, technical difficulties resulted in imprecise determination of the detonation time (of the order of few hundreds milliseconds). Therefore, we observed some inconsistencies in reciprocal times of reversed traveltime branches. We attempted to apply suitable corrections for shot timing of individual seismic sections based on the analysis of the residuals (time differences of the same phase in reversed sections) for all pairs of shots where reciprocal traveltimes of some phase could be measured. The corrections were calculated with a goal to minimize total reciprocal residuals for all 14 explosions. After this operation, the maximum residuals in reciprocal points decreased from ∼230 to ∼100 ms which is an acceptable result.

The resulting seismic sections from SP15701 to SP15714 are displayed in Fig. 4 using a reduction velocity of 8 km s^{-1}. For presentation purposes all traces have been subject to an Ormsby 2–18 Hz bandpass filter, followed by amplitude normalization.

4 DESCRIPTION OF THE OBSERVED WAVEFIELD

The observed wavefield contains all of the main phases needed to construct the velocity model. Our high quality seismic records (Fig. 4) generally allow reliable phase correlation of refracted *P*-wave phases from the sedimentary and deeper crustal layers (P_{sed}, P_g and P_{ov}) which are easily identified, as well as reflections (P_cP, from crustal interfaces; P_MP, from the bottom of the crust) and refractions (P_n) from the Moho and mantle refractions (P_{mantle}) and reflections (P_1P, P_2P).

The above phases were correlated in the seismic sections and resulting traveltime curves served as the basis for determination of seismic velocity distribution and depths to velocity discontinuities in the crust and upper mantle.

The near-offset refractions from sedimentary layer P_{sed} display pronounced variation in offset range and in their apparent velocity because of the different depth of sedimentary basins and different Vp velocity in PT, DG and BU in the central part of the profile. These phases are practically absent in record sections from two northern shots. Apparent velocities of P_{sed} are highest in the central part of the profile (SP15707), where values of around 5.0 km s^{-1} are observed. Due to higher content of salt in Devonian sequences, the P_{sed} in the PT area shows a little higher apparent velocities of ∼4.0 km s^{-1} compared to the DG, where apparent velocities are ∼3.0 km s^{-1}. The maximal intercept time of P_g in PT basin is less than 1 s (reduce time). In the DG it increases from 2.5 s at SP15708 to ∼3 s at the southern end of the profile, where the sedimentary cover is thicker and reaches depths of 13 km.

The strongest arrivals from the crystalline crust are the Pg phase, with apparent velocity of ∼6.0 km s^{-1} (Fig. 4, SP15701–SP15714) at the distances 30–130 km, and P_MP phase (reflection from the Moho boundary), visible in secondary arrivals in the offset range of 30–130 km. In some places, the apparent velocity of P_g increases substantially (Fig. 4, SP15704 offset ∼150 km; SP15705 ∼90 km; SP15707 ∼ 110 km; SP15708–SP15712 ∼60 km all to SE, and SP15708–SP15710, 50–100 km to NW). This phase usually shows a remarkably "ringing" character with 1.5–2.5 s long coda (e.g. Fig. 5, SP15702: offset 15–125 km; SP15713: offset-100 to −50 km; SP15714: offset −110 to −65 km). In many cases, strong crustal refractions continue as later arrivals up to large offsets of 180–220 km (e.g. SP15701, SP15702, SP15703 and SP15709). Modelling of these phases gives valuable information about lower crustal velocities and allows to estimate the maximum velocity in the lower crust.

Arrivals from within crystalline crust include several reflection events, which are interpreted as originating as reflections from boundaries between upper, middle and lower crust, based upon the velocity changes modelled at the discontinuities. Phases reflected from the bottom of the upper crust are observed in most shot records at offsets from 50 to 120 km. Reflections from the high velocity lower crust are often observed at offsets of about 90 to 200 km. This phase is clear in first two shots (SP15701 and SP15702) and in the part of the profile starting from the BU along the DG (SP15706 and SP15714).

Reflections from the Moho (P_MP) are visible beginning at offsets of ∼100 km on most of the record sections. Particularly clear P_MP phases are recorded in the sections of SP15701, SP15702, SP15707, SP15708 and SP15710 for 120–250 km offsets (Fig. 4).

Very clear Pn phase in first arrivals is observed in all shot gathers except SP15713 at offsets larger than 150 km, showing apparent velocity of ∼8.2 km s^{-1}. In the central part of the profile (Fig. 4, SP15706–SP15710), the Pn phase is observed in both directions.

A strong seismic phase from the lower lithosphere (P_{mantle}) is observed as a later arrival in several record sections (SP15701–SP15705 at offsets of 350–600 km, illustrated in Fig. 4). In the record sections SP15710 and SP15711 we observe this phase in opposite direction at offsets of ∼300 km at around 9 s reduced time. It is characterized by high apparent velocity of 9 km s^{-1} and more than 1 s long coda.

Mantle phases (P_{mantle}) are observed in later arrivals in the several sections, e.g. SP15703, SP15708 and SP15710 (Fig. 4).

5 SEISMIC MODELLING

5.1 Ray-tracing modelling

For modelling of the seismic data, two methods were used. First, ray-tracing trial-and-error modelling was performed. Next, analysis of the amplitudes of the recorded phases was done using full waveform calculation with a finite-difference (FD) code.

The trial-and-error forward modelling was done using the SEIS83 package (Červený & Pšenčík 1984) with the graphical interface MODEL (Komminaho 1998) and ZPLOT (Zelt 1994). The algorithm uses the ray method for tracing of ray paths and calculation of traveltimes as well as the synthetic seismograms in the high-frequency approximation. A model consists of layers with smoothly varying velocities, separated by discontinuities. In each layer, the *P*-wave velocity is parametrized on an irregular rectangular grid and interpolated by bicubic splines. In this study, geological and geophysical data from over a dozen boreholes located near the

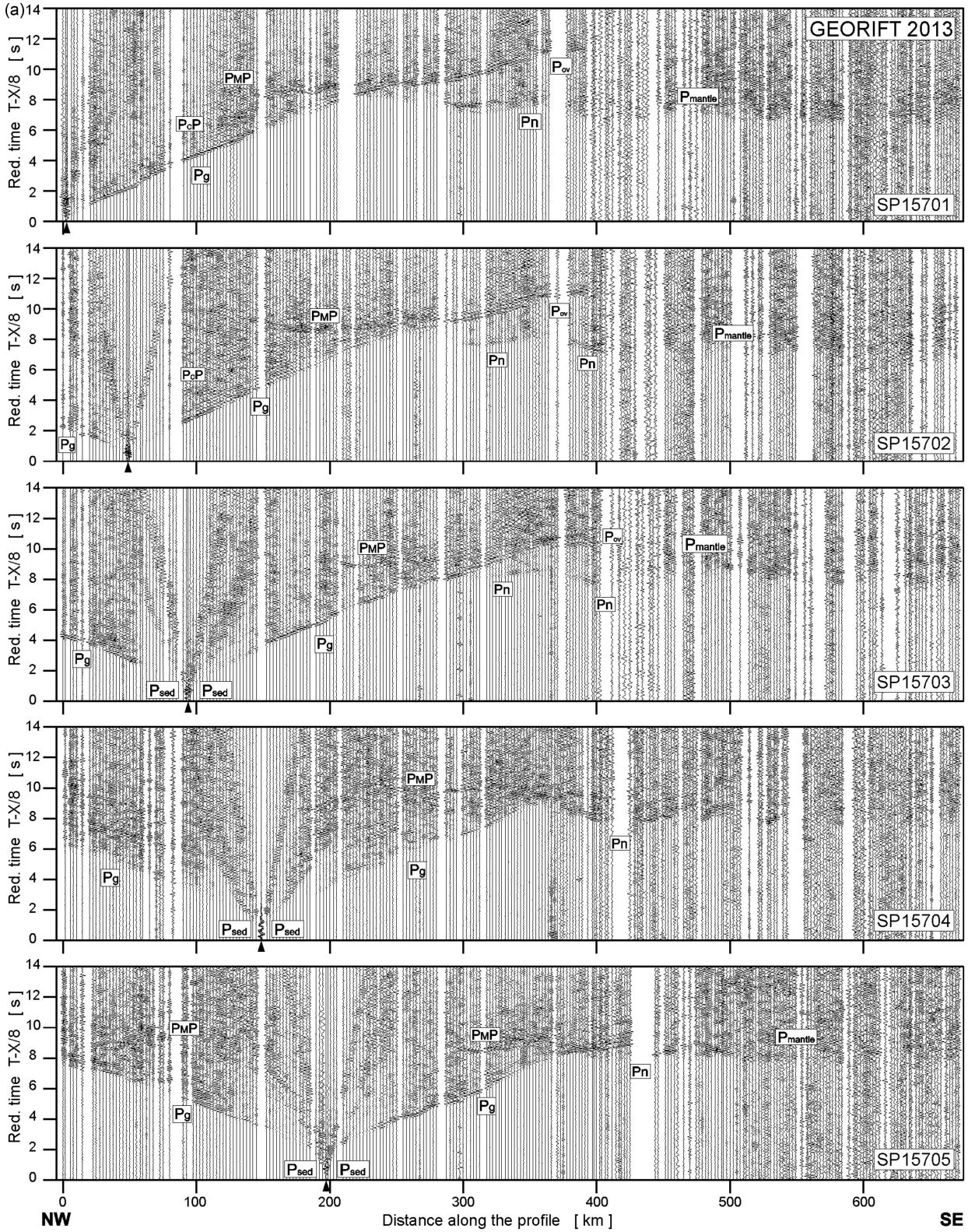

Figure 4. (a, b, c) Examples of trace-normalized, vertical-component seismic record sections for *P* waves (SP15701–SP15714). Abbreviations: P_{sed}, seismic refractions from sedimentary layers; P_g, refractions from the upper and middle crystalline crust; P_{ov}, overcritical crustal phases; P_cP, reflections from the mid-crustal discontinuities; P_MP, waves reflected from the Moho boundary; P_n, refractions from the sub-Moho upper mantle; P_{mantle}, *P*-wave phases from the upper mantle. The reduction velocity is 8.0 km s^{-1}.

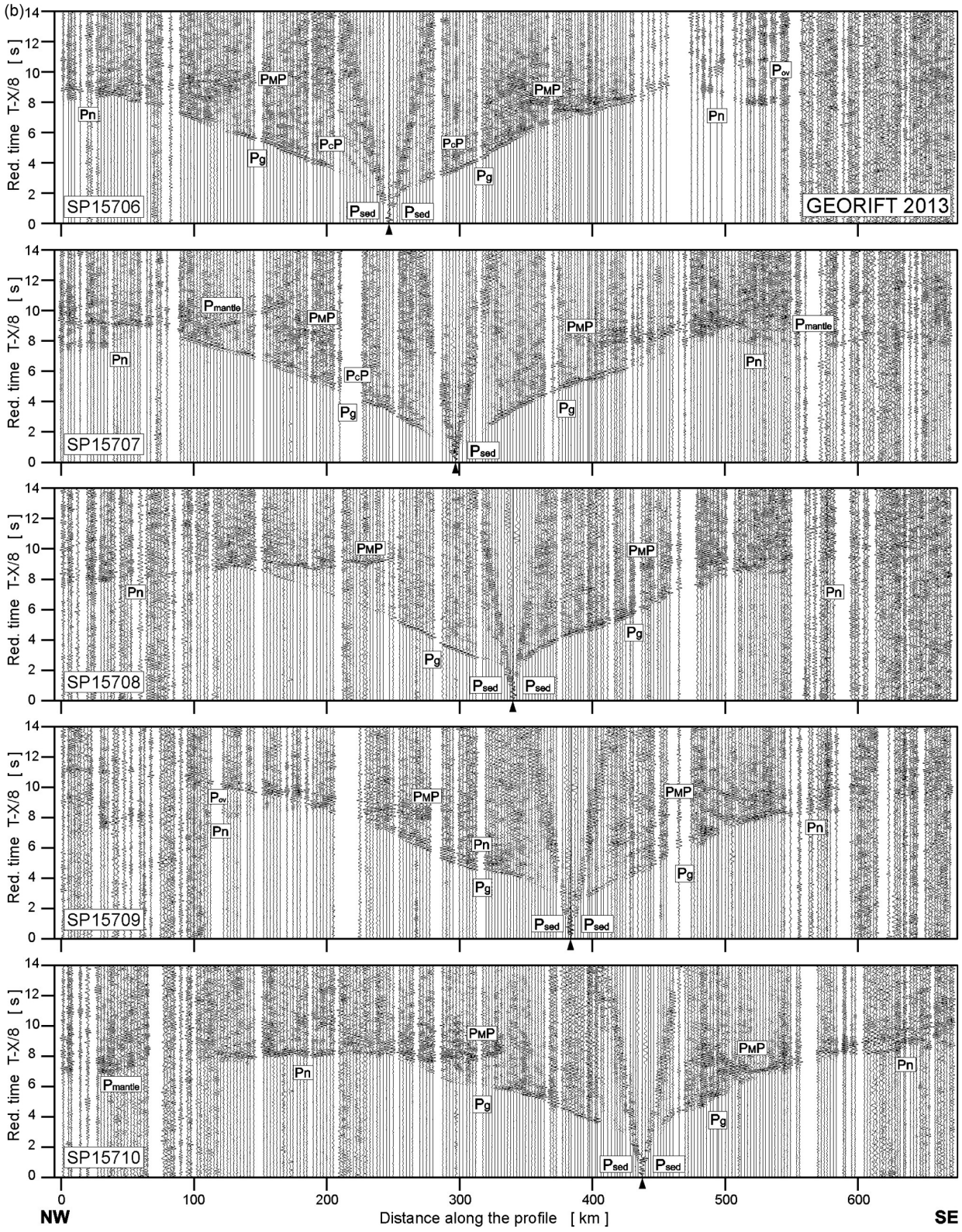

Figure 4 (*Continued.*)

profile and velocity data from shallow seismic reflection and refraction investigations were used, when available, to constrain the velocity distribution in the uppermost crust during preparation of the initial model. The model was iteratively modified in order to minimize the traveltime misfit and to obtain similar amplitudes of synthetic and observed data. Amplitude provides important constraints on the velocity gradients and contrasts at the discontinuities. The modelling was iterated until a good agreement between the observed and calculated traveltimes and amplitudes for the main phases was obtained (Fig. 6). Examples of ray-tracing forward modelling, as well

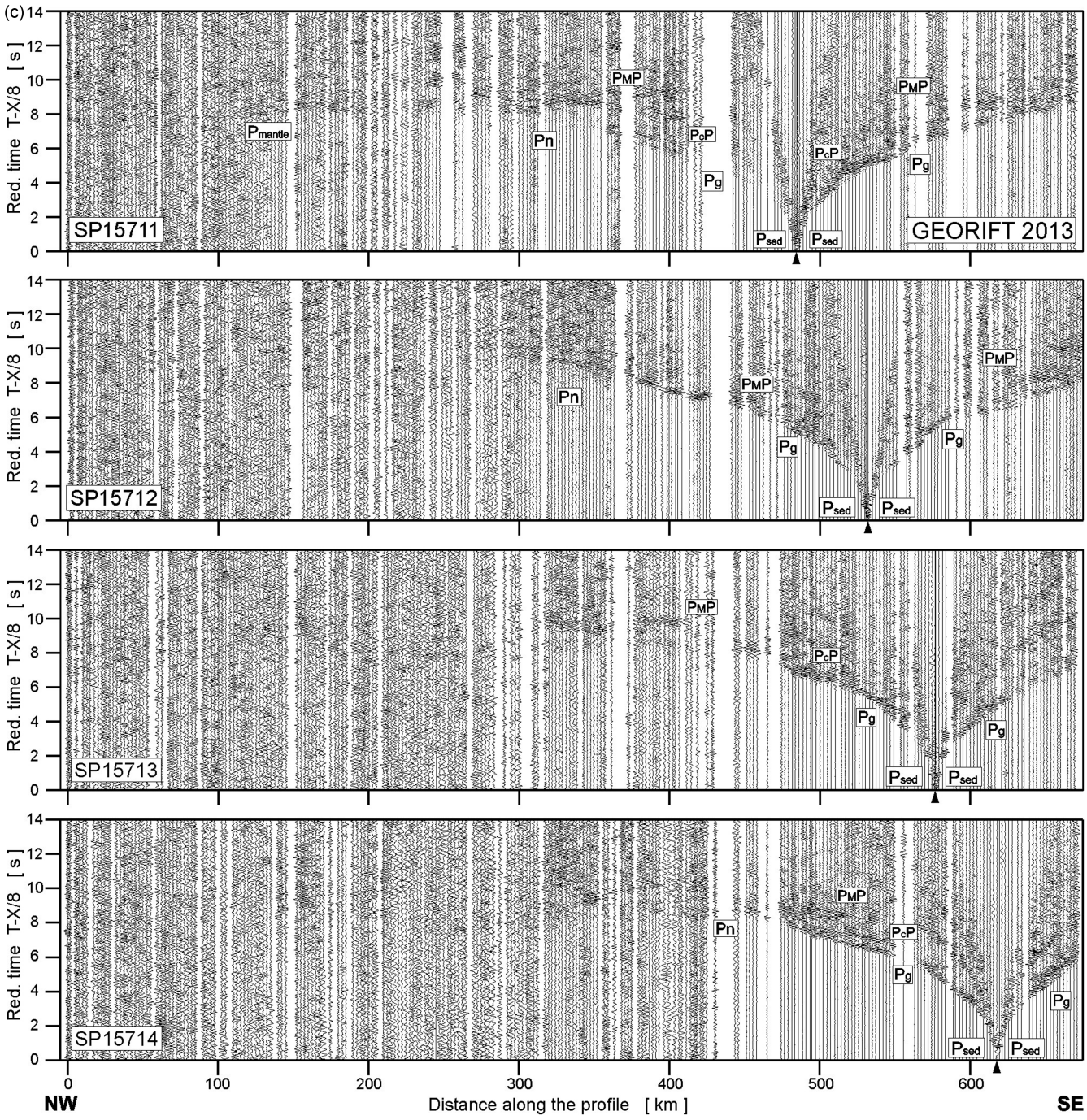

Figure 4 (*Continued.*)

as examples of full waveform synthetic seismograms, are shown in Fig. 7.

5.2 Full waveform synthetic sections

Full waveform synthetic sections were calculated with Tesseral package (Kostyukevich *et al.* 2000). It uses fast and accurate computational scheme based on the FD method, which allows for efficient modelling of the wavefield in an arbitrarily complex geological medium. An initial model consists of ordinary polygons, layer-like polygons, top and bottom type horizons and polylines such as faults. In this work, we used a different algorithm for conversion of the velocity model into the Tesseral input format compared to our previous WARR seismic profiles along PANCAKE (Starostenko *et al.* 2013a) and DOBRE-4 (Starostenko *et al.* 2013b). In the previous studies, the velocity model was expressed as a grid with 500 m horizontal and 100 m vertical spacing and imported to Tesseral package as gridded data. This time, we used a different approach: the final ray-tracing velocity model (Fig. 6) was converted layer by layer to polygons with the same parameters. Corresponding *P*- and *S*-wave velocities were defined with gradient as in the velocity model from ray-tracing. Subsequently, the polygons were visually edited and smoothed. Similarly as in the ray-tracing model, the surface topography was also taken into account. Several seismic

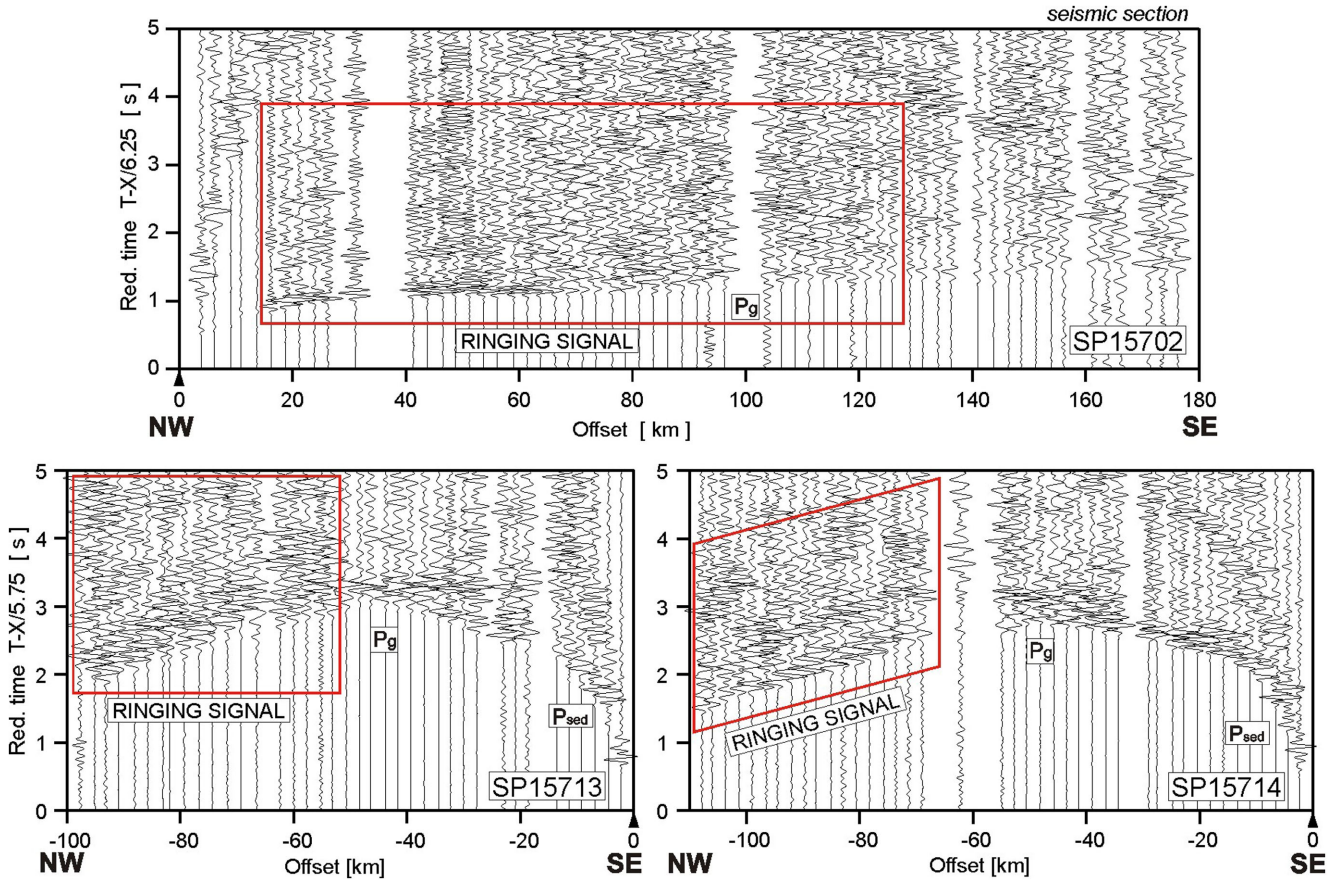

Figure 5. Examples of remarkable 'ringing' P_g phases on fragments of trace-normalized, vertical-component seismic record sections (SP15702, SP15713 and SP15714). The reduction velocities are 6.25 and 5.75 km s^{-1}, respectively. The ringing phases are marked by red frame. Abbreviations are as in Fig. 4.

source wavelets were tested during the experiments, the Puzyrev wavelet with 8 Hz frequency showed the best coincidence with observed wave field at least in the near-offset zone. We observed a very good agreement of synthetic sections with recorded data, which also confirms high accuracy of the velocity model, as discussed further in the article.

Due to the large volume of input data, the computations were performed on a grid of computers using parallel computation algorithms (Kolomiyets & Kharchenko 2008).

Comparisons of the calculated full waveform synthetic sections with seismic record sections as well as the ray diagrams for SP15701, SP15703, SP15705, SP15707, SP15708, SP15710 and SP15712 are presented in Figs 7(a)–(g), respectively.

We can see differences in synthetic sections calculated by ray-tracing and by full waveform method, for example, at 200–400 km in Fig. 7a. This can be explained by the differences in the approaches used in the calculations. The algorithm, implemented in SEIS83 has significant limitations as it solves the eikonal equation (ray theory approximation) rather than full wave equation.

Full-waveform synthetic seismograms obtained by the FD method take into account the propagation of all wave types, including converted and multiple ones. That yields a picture closer to the result of an actual experiment. Indeed, when comparing full waveform synthetic sections with actual records, we can see a good correspondence in most sections, also for the first arrivals of P_n in the interval of 200–400 km (Fig. 7a) mentioned above, which demonstrates the advantages of using full-wave simulation for calculating synthetics.

5.3 Crustal model

The initial model was prepared based on the available data about the uppermost crustal structure—results of shallow reflection seismic, geological studies and velocity measurements from 16 boreholes (reaching 1.2–6 km depth), which are among the total number of the boreholes (40) shown on the geological section in Fig. 3, located in the vicinity of the profile at up to 1.9 km distance. More complete information was available on the Ukrainian side than on the Belarusian one. The thickness of the sedimentary layer varies along the profile from ∼0.3 km in the NW to ∼13 km in the SE. The Vp velocities in the sediments increase substantially with depth, from 1.8 km s^{-1} in the near-surface layers to 5.8 km s^{-1} in the deepest sedimentary sequences. At 90–120 km distance along the profile, in the NW part of the PT, high velocity layers were found in the sediments: Vp = 4.3 km s^{-1} at ∼0.5 km depth and Vp = 5.5 km s^{-1} at ∼2 km depth.

In our final model (Fig. 6), the velocity distribution in the uppermost crust is in large part based on the information comprised by the initial model, but in some places the structure and depth of sedimentary layers were modified during modelling in order to fit the upper crustal traveltime data from the GR'13 profile.

The top of the crystalline crust, with *P*-wave velocities of 6.2-6.1-6.25 km s^{-1}, is located at ∼0.3 km depth at the NW end of the profile and slopes gently to 2–5 km at 440 km distance. More to SE, it abruptly submerges to over 8–10 km depth, reaching ∼13 km at the SE end of the profile.

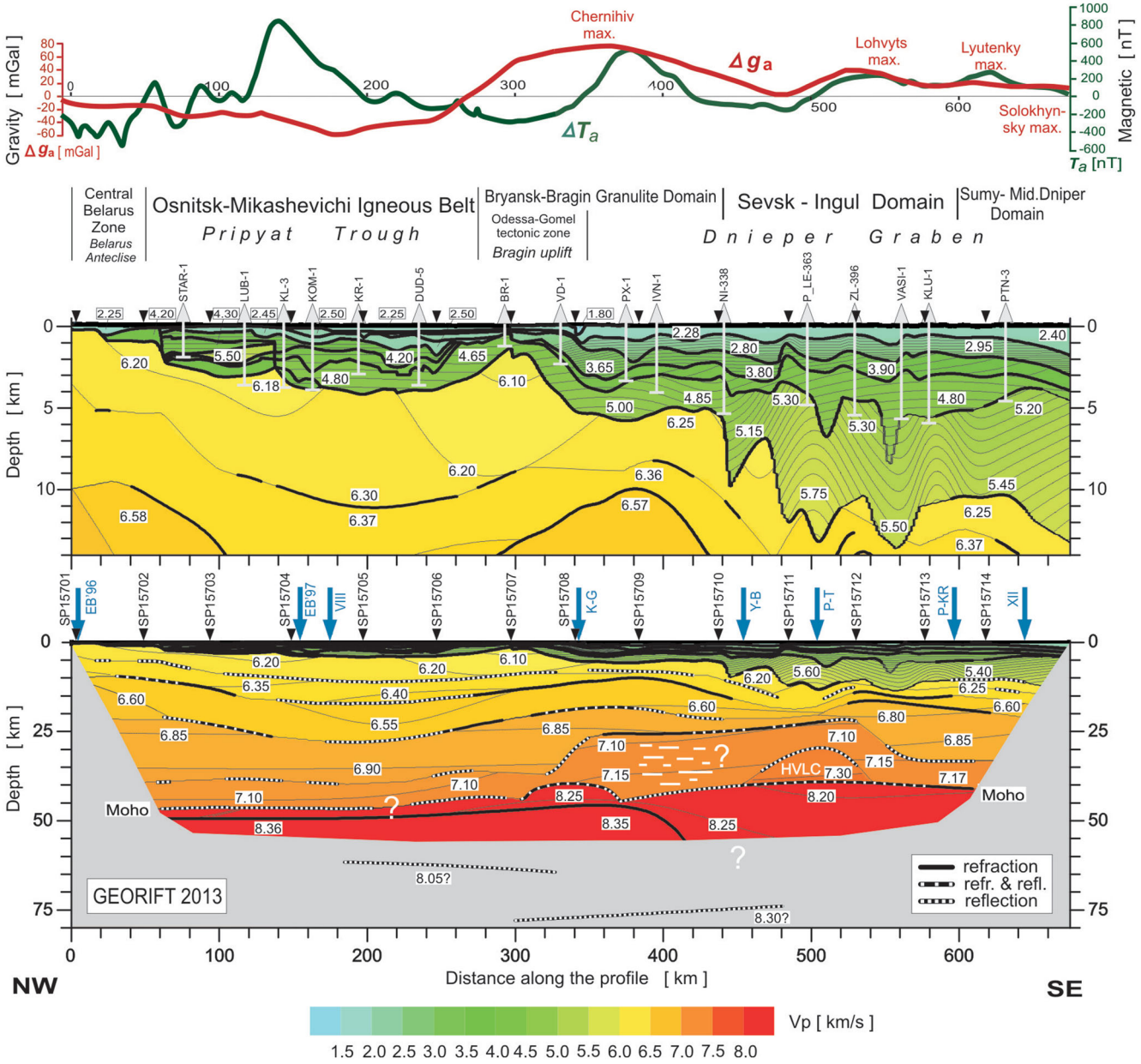

Figure 6. 2-D model of seismic *P*-wave velocity in the crust and upper mantle derived by forward ray-tracing modelling using the SEIS83 package (Červený & Pšenčík 1984) along the GEORIFT 2013 profile. Thick, black solid and dashed lines represent major velocity discontinuities (interfaces). Colours represent velocity isolines with values in km s^{-1} shown in white boxes. The position of tectonic units is indicated. Arrows show positions of shotpoints. Blue arrows show intersections with other profiles. Abbreviations are as in Figs 1 and 3. Vertical exaggerations are ~11:1 for upper part of the model and ~2.4:1 for the whole model. Bouguer gravity and total magnetic field anomalies along the profile are shown in top diagrams (Starostenko *et al.* 1986; Pashkevich *et al.* 2014).

The upper and middle crystalline crust, reaching depths of 17–27 km, consists of three layers with small velocity contrasts at the discontinuities, therefore the locations of the boundaries between them is not well documented. The uppermost layer shows *P*-wave velocities of 6.1–6.25 km s^{-1}, while the deeper layers are characterized with Vp of 6.35–6.4 km s^{-1} and 6.5–6.6 km s^{-1}.

The lower crust in its uppermost parts shows velocities of 6.8–6.9 km s^{-1}. In the deeper parts of lower crust, with the top at 36–39 km depth up to ~320 km distance, *P*-wave velocities of ~7.1 km s^{-1} are observed (Fig. 6). Between 320 and 500 km distance, this layer, with slightly elevated velocities (7.1–7.15 km s^{-1}) becomes substantially thicker, with well documented top at 22–26 km depth (SP15708-SP15712). Our data do not allow for reliable determination of the internal structure of this thick lower crustal fragment. It seems, however, that existence of lower, more 'typical' velocities just below the thin high-velocity layer at the top of the lower crust, may be an alternative solution, acceptable in terms of the fit to observed high reflectivity. Between 460 and 535 km distance, a body with Vp of 7.3 km s^{-1} was observed just above Moho boundary, but it was modelled based on synthetic seismograms only.

5.4 Moho boundary and upper mantle

The Moho boundary in the NW part of the model (up to 290 km distance) is well documented by P_MP reflections (Figs 4 and 7, SP15701–SP15703, SP15705–SP15709). In 310–370 km distance

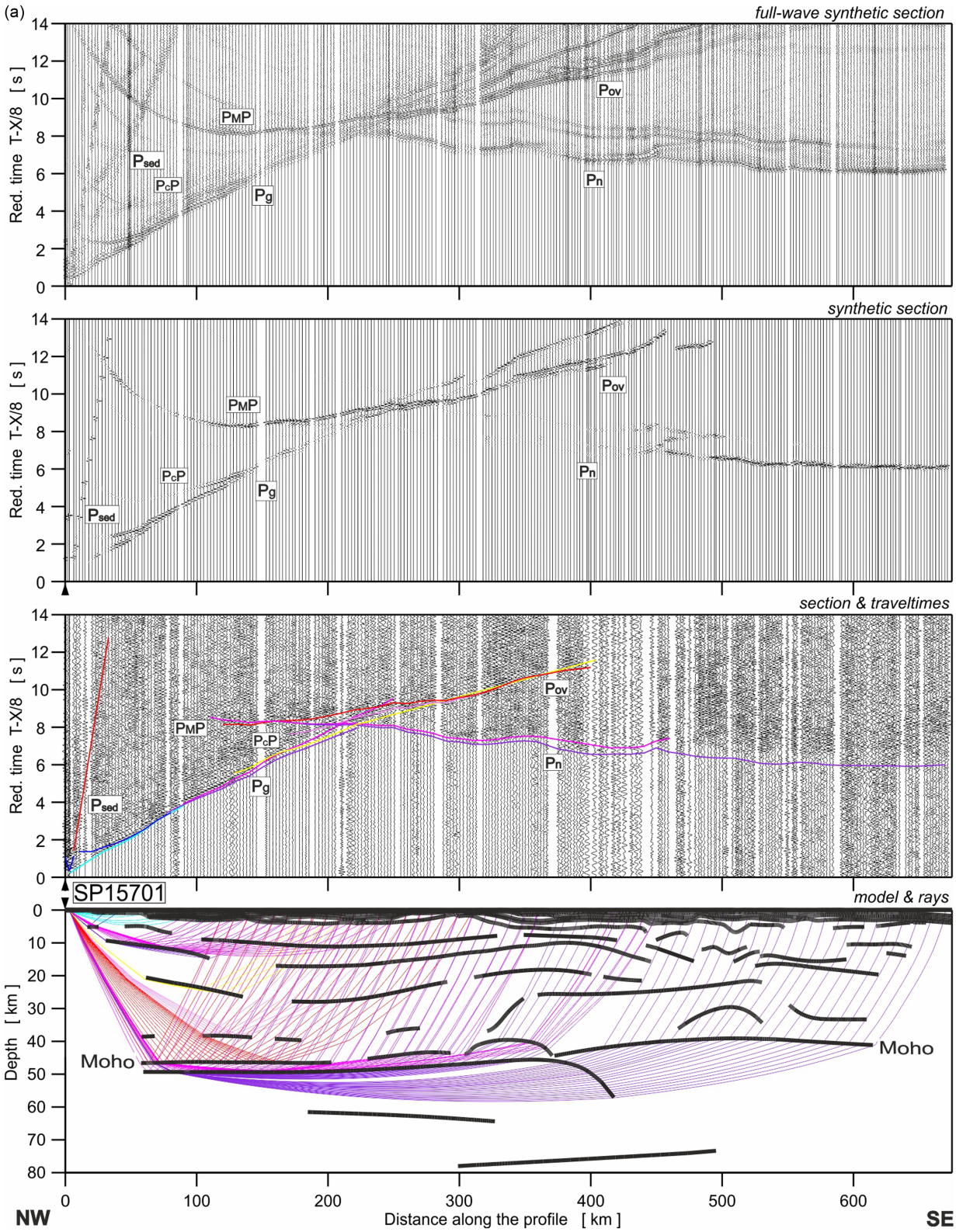

Figure 7. Examples of seismic modelling along the GEORIFT 2013 profile: (a) SP15701, (b) SP15703, (c) SP15705, (d) SP15707, (e) SP15708, (f) SP15710, and (g) SP15712. Seismic record sections (amplitude-normalized vertical component) of *P* waves with theoretical traveltimes calculated using the SEIS83 ray-tracing technique. *P*-wave data have been filtered using the bandpass filter of 2–15 Hz and displayed using the reduction velocity of 8.0 km s^{-1}. Full-wave synthetic seismograms (second diagram) using TESSERAL program (Kostyukevich *et al.* 2000). Synthetic seismograms (third diagram) and ray diagram of selected rays using the SEIS83 (bottom diagram). All examples were calculated for the model presented in Fig. 6. Other abbreviations are as in Fig. 4.

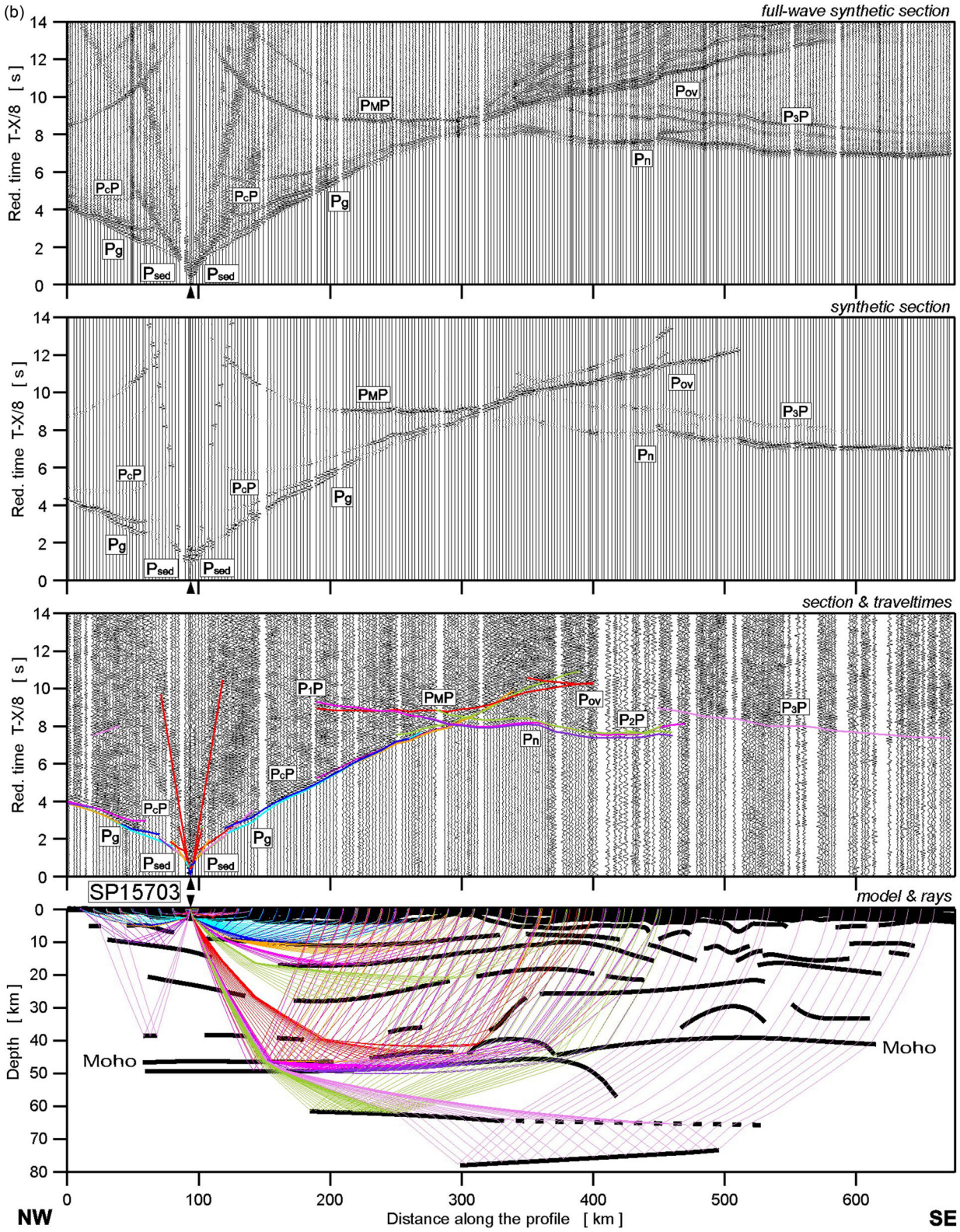

Figure 7 (*Continued.*)

range, a ∼5 km uplift of the Moho discontinuity is observed—from 40 to 35 km in the middle part (SP15707–SP15711), and more to the SE Moho gets deeper to ∼44 km at 370 km distance, as documented by modelling of the P_MP and P_n phases. Further to SE, Moho discontinuity was found at ∼39 km at 505 km distance and at 41 km depth beneath the SE end of the profile. In this part, besides the P_MP phase visible on many sections, also the P_n phase can be observed for some shot points (SP15708, SP15710 and SP15711).

In the NW part of the model, the mantle refraction seems to originate from a shallow, sub-Moho mantle discontinuity, with Vp

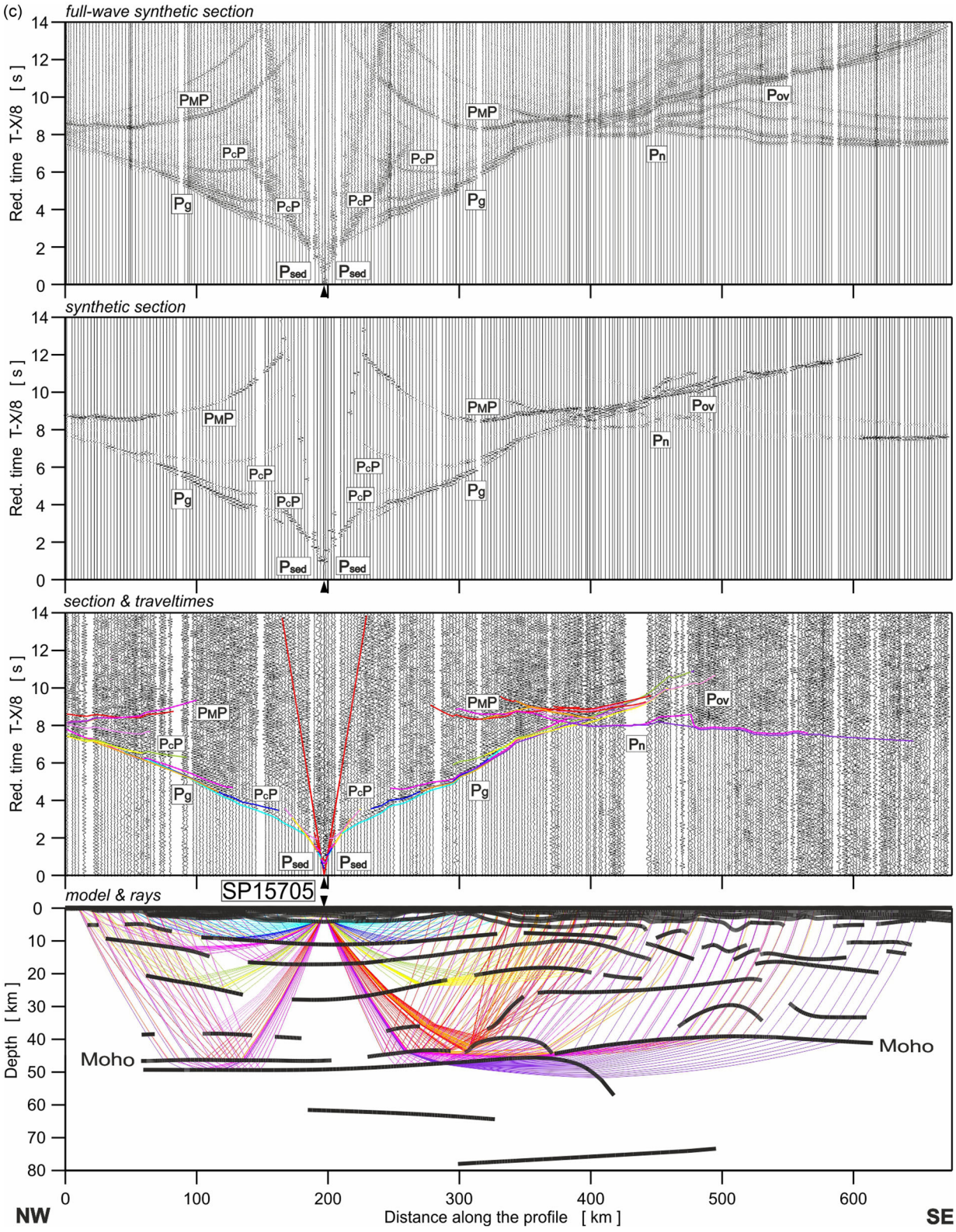

Figure 7 (*Continued.*)

of ~8.35 km s^{-1}. It is observed in sections for SP5701 to SP15707, as a very clear phase up to 490 km. In other parts of the profile we can also observe P_n phase, but its arrivals are not easy to correlate.

The depth of the sub-Moho mantle discontinuity decreases from 50 to 44 km in the distance range 90–410 km, and further to the SE increases to 56 km. This discontinuity is documented only by few reflections, for example, at sections SP15702 and SP15705 (Figs 8a and b). Additionally, we prepared comparison of P_n traveltimes modelling for two possible solutions, with Vp ~ 8.35 km s^{-1} just below Moho boundary (Fig. 8c) and other one, presented in our

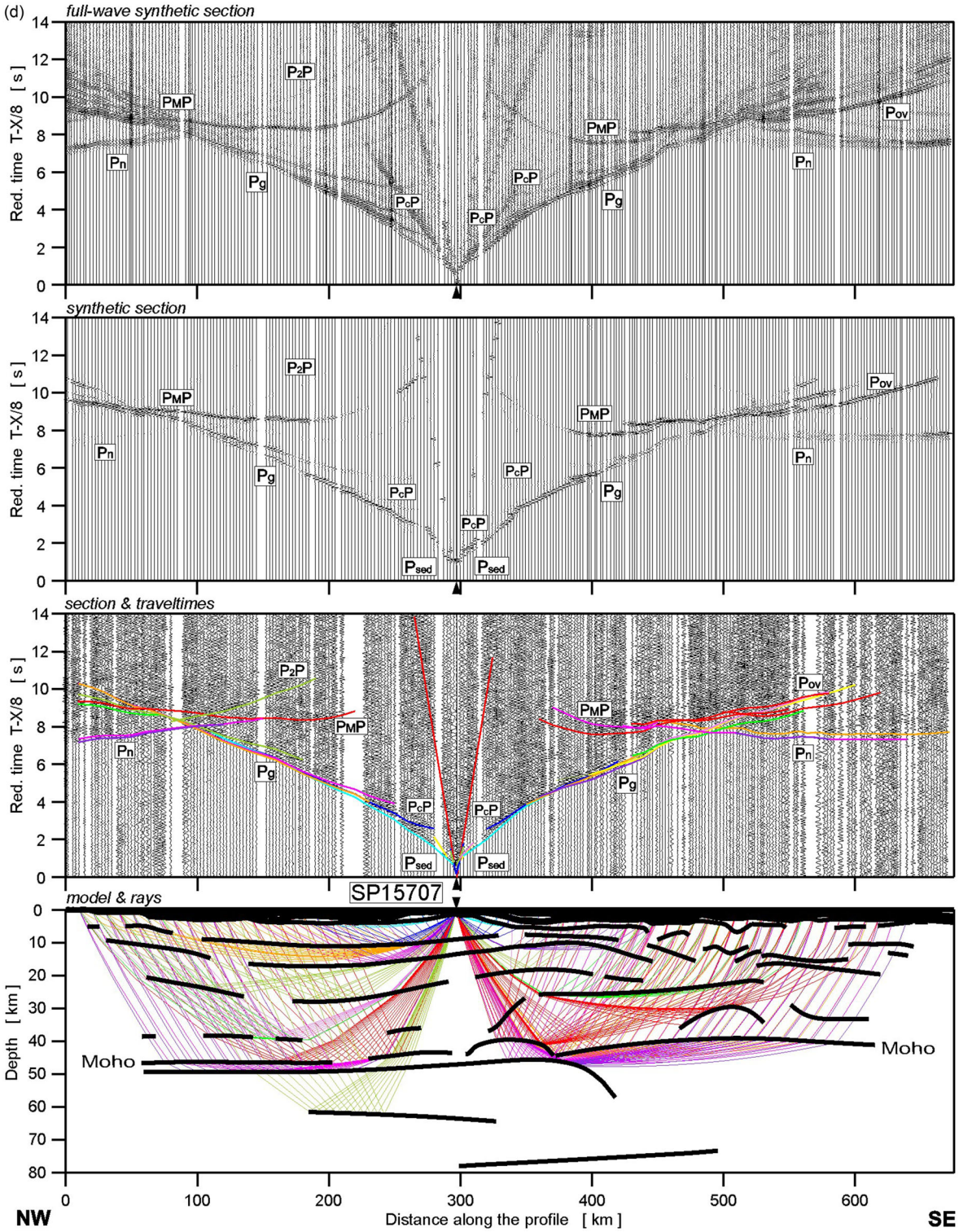

Figure 7 (*Continued.*)

model (Fig. 6), with Moho (Vp ∼ 8.2–8.25 km s^{-1}) and high velocity layer below shallow sub-Moho boundary (Fig. 8d). In the 'trial and error' modelling process, different solutions were tested. It was problematic to prepare a model producing high apparent velocity calculated arrivals which match the observed first pulses for lower lithospheric waves. The solution was to use a high velocity layer (Vp ∼ 8.35 km s^{-1}) with a relatively low gradient. The resulting traveltimes have appropriate apparent velocity, but required some time delay. It is possible to imagine other solutions but in our opinion, the GR'13 model is, however, more likely. The modelling of the reflector was also partially based on the EUROBRIDGE'97 model (Thybo *et al*. 2003), where, at intersection with GR'13 profile, it seems to be well documented by strong reflections (the authors suggest also alternative possibility—a zone of large velocity gradient in the upper mantle—which in our opinion seems very difficult to model).

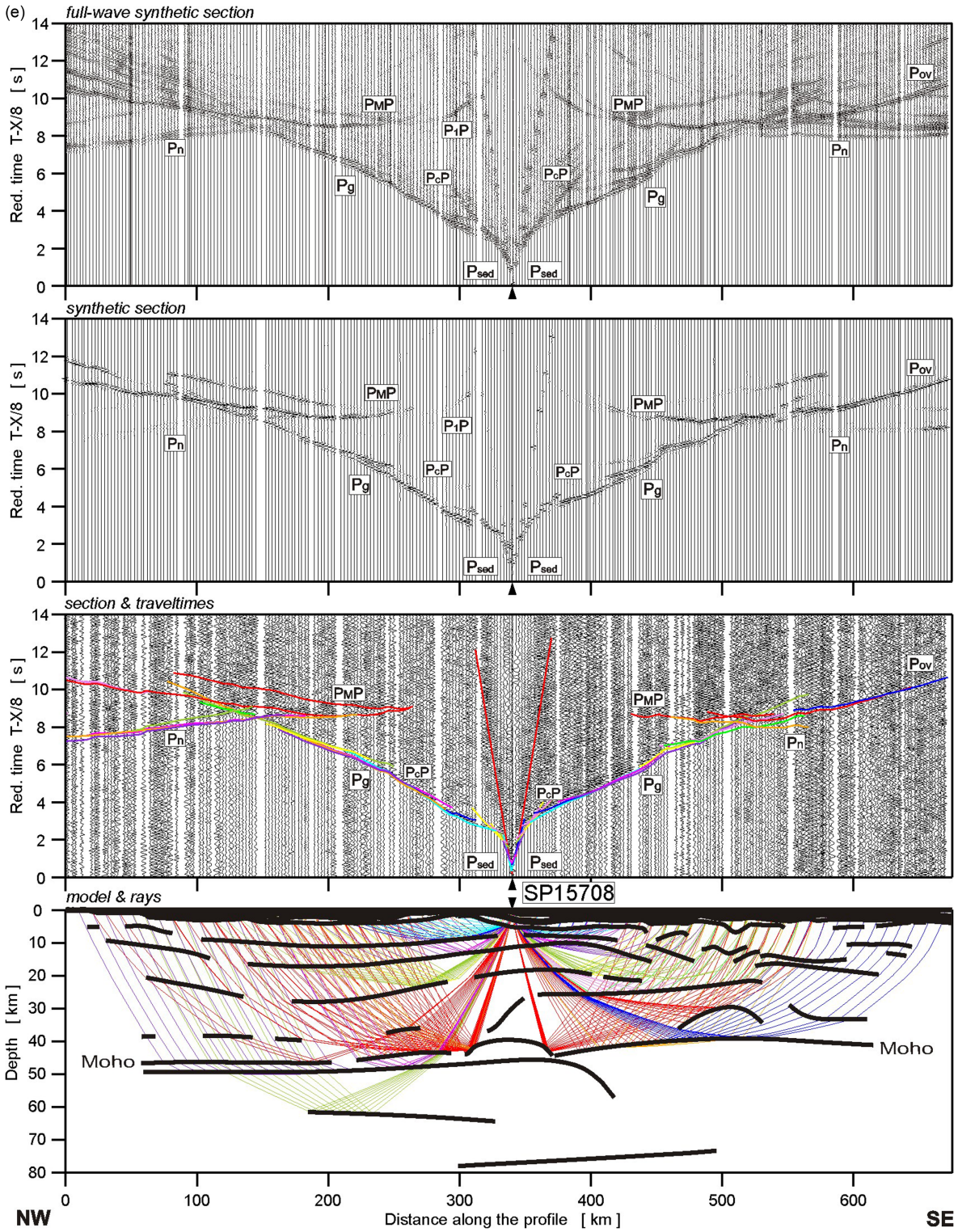

Figure 7 (*Continued.*)

High amplitude mantle arrivals in the SP15707 section (Fig. 4, at 100–180 km distance and 9–11 s reduced traveltime) can be interpreted as reflections from the mantle discontinuity at depth of ∼62 km in the distance range 180–320 km. However, velocity contrast assumed in the model does not produce sufficiently strong amplitude of this phase in synthetic seismograms.

Strong reflected phases visible in later arrivals in SP15702 and SP15703 sections in the SE part of the profile (distance range 450–670 km) may originate from a reflecting discontinuity at ∼77 km depth located in 300–480 km distance range. Here, similarly, velocity contrast proposed in the model did not produce sufficiently strong amplitudes of synthetic seismograms.

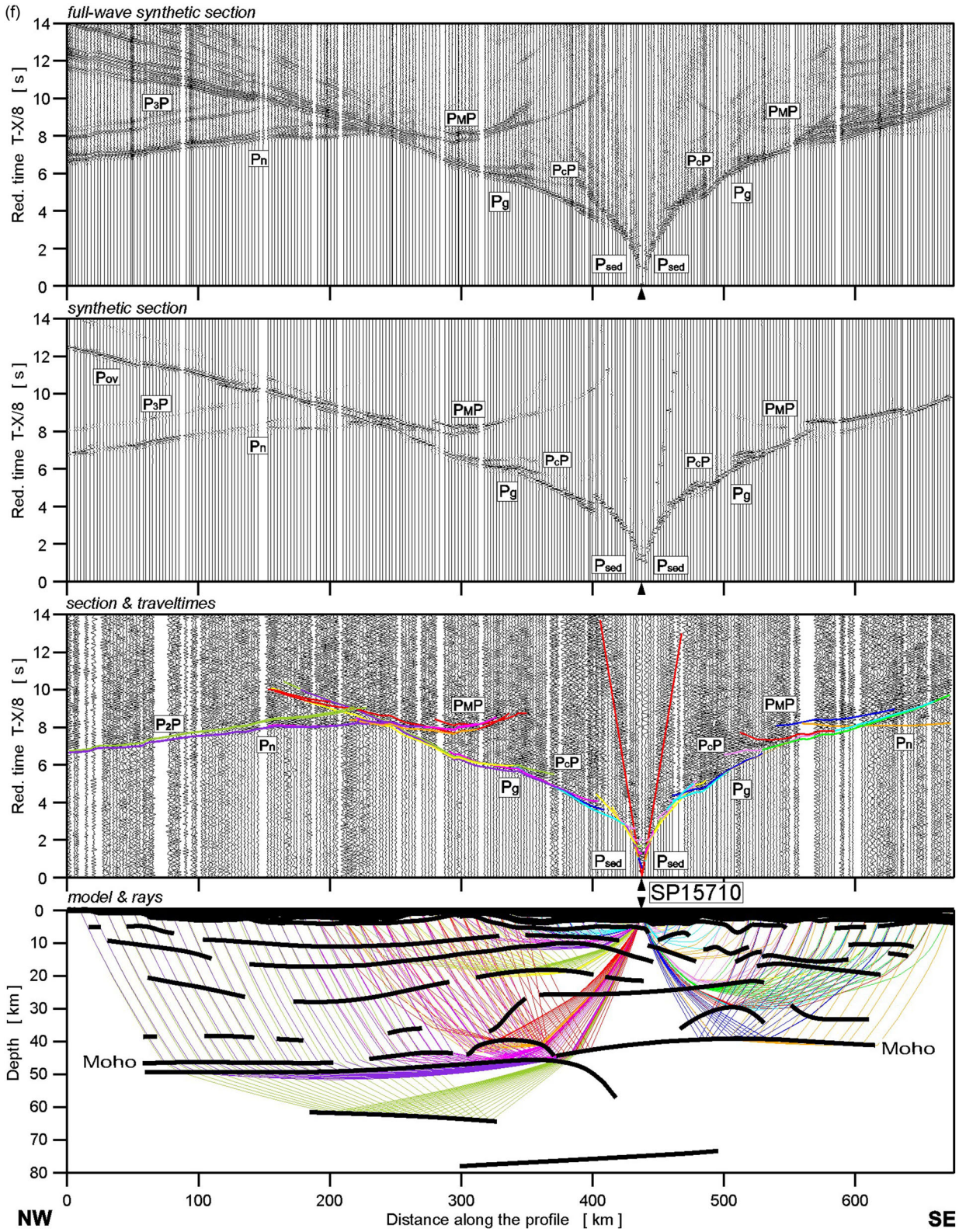

Figure 7 (*Continued.*)

5.5 Resolution analysis

During the experiment, the shot times and locations for shots and receivers were measured very precisely, using modern GPS techniques, in the order of 1 ms and tens of meters, respectively. Unfortunately, there were technical issues caused by the using of two explosion techniques during the shooting: detonating cable and electrical fuses, that leaded to unexpected shot delays. Besides these timing errors, uncertainties of velocity and depth in the model obtained using the ray tracing technique result mainly from the uncertainties of

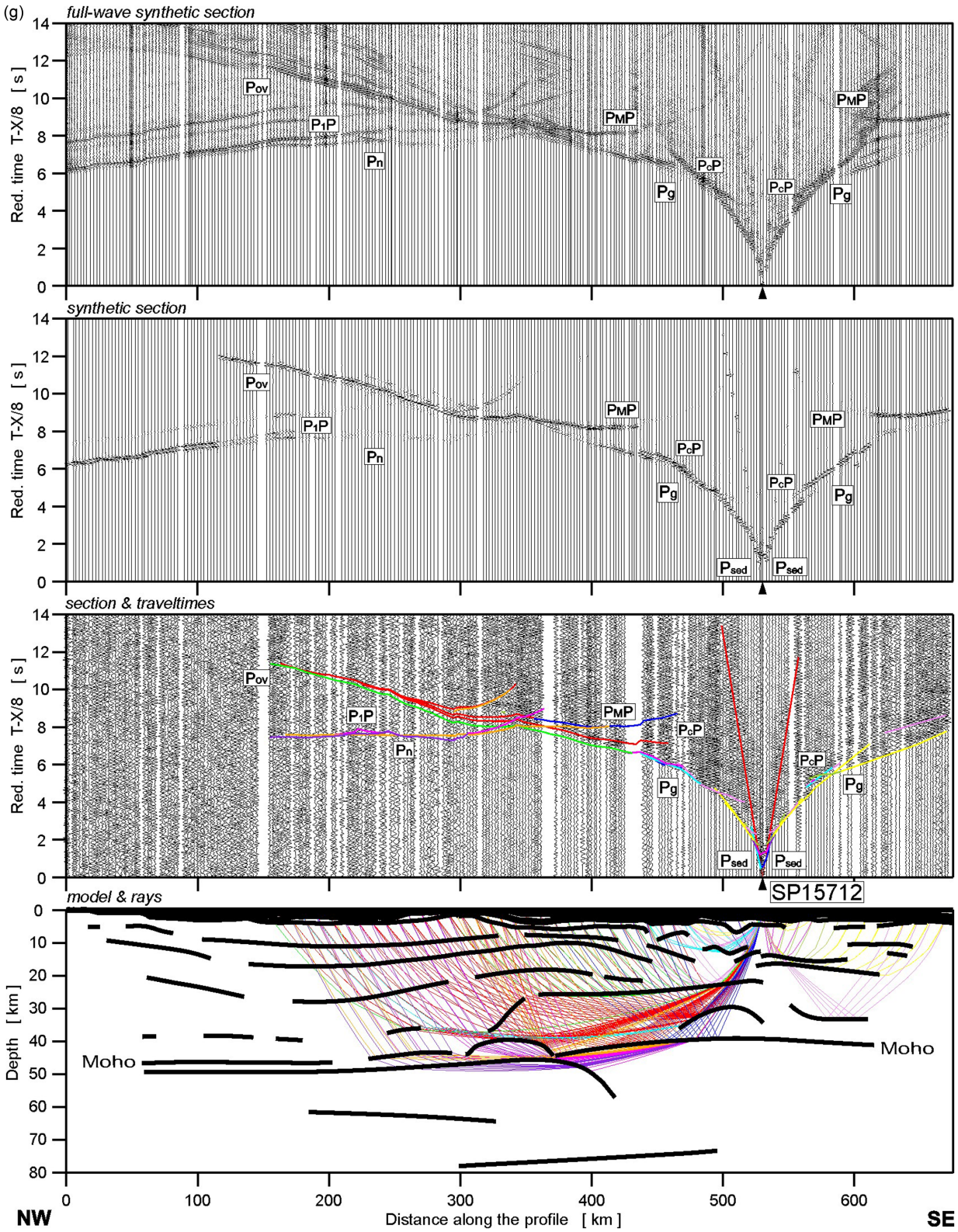

Figure 7 (*Continued.*)

subjectively picked traveltimes, which is of the order of 0.1 s. However, the accuracy increases with increasing quality and amount of data (number of shots and receivers, effectiveness of sources, signal-to-noise ratio, check of reciprocity of the traveltime branches, ray coverage in the model).

Good quality of the data allowed us to construct a velocity model that fitted the observed traveltimes for both refracted and reflected waves with good accuracy. Several studies (e.g. Janik *et al.* 2002; Grad *et al.* 2003, 2006a,b; Środa *et al.* 2006; Janik *et al.* 2009) show that in the areas with good ray density, the accuracy of our model

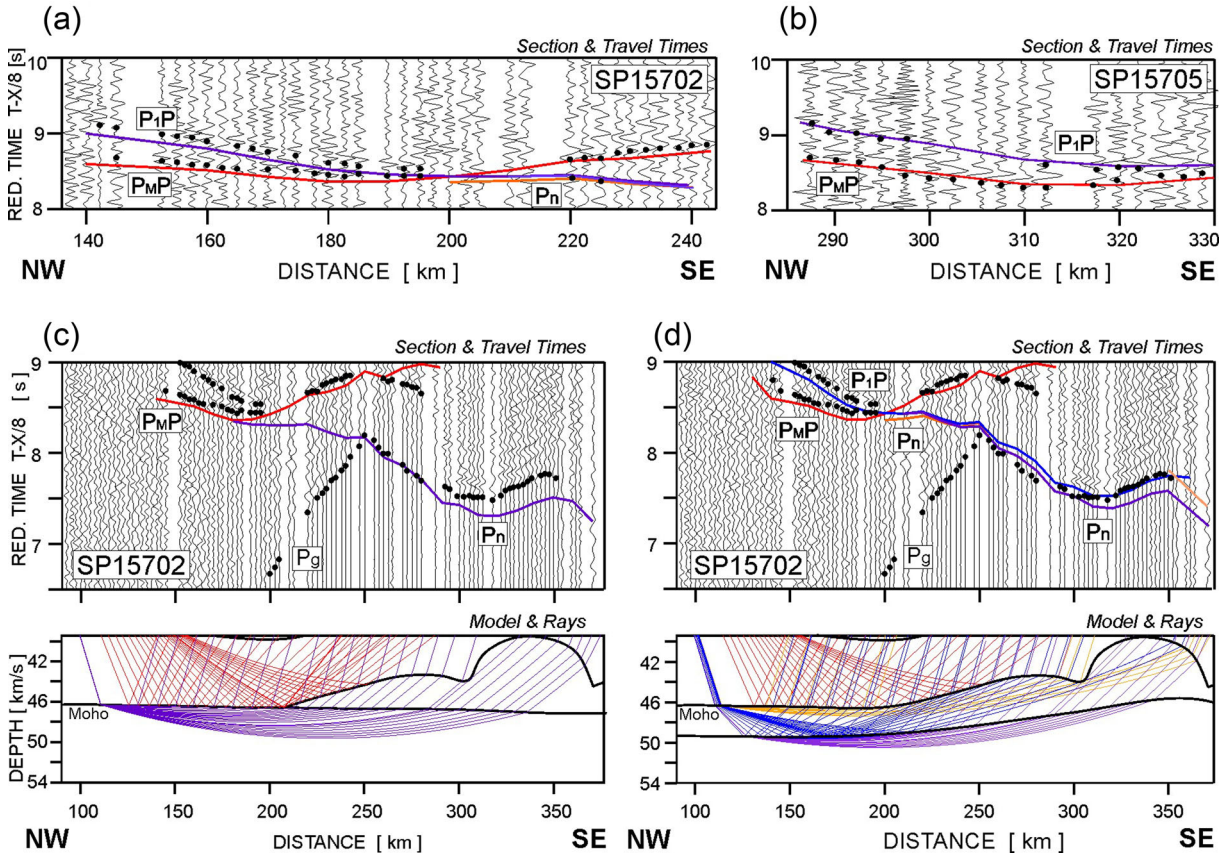

Figure 8. Detailed examples of seismic modelling of the crust–mantle structure: for SP15202 (a)—two reflectors, Moho and sub-Moho; same for SP15705 (b); comparison of P_n theoretical traveltimes with seismic section SP15702 for model with Vp~8.35 km s^{-1} present below Moho boundary—too early (c); for model (Fig. 6) with Vp~8.35 km s^{-1} present below sub-Moho boundary (d). Abbreviations are as in Fig. 4.

is better than ±0.1 km s^{-1} and ±2 km concerning respectively *P*-wave velocity and Moho depth. Diagrams showing theoretical and observed traveltimes for all the phases along the profile, ray coverage and traveltime residuals from forward modelling are shown in Fig. 9. The RMS values are acceptable, being 0.19 for the crust, and 0.28 for P_MP and 0.25 for P_n phases. The RMS value for refracted phases in the crust is 0.09 while for reflections it is 0.28. The overall RMS value for 4062 picks is 0.21. Thus, it is concluded that calculated traveltimes for refracted phases in the crust fit better experimental arrival times than these for reflected phases. The elements of the crustal structure based on modelling of traveltimes of refracted rays, particularly the *P*-wave velocity field, is relatively best determined.

6 INTERPRETATION AND DISCUSSION

Rifting and associated magmatic activity were widespread in Late Palaeozoic and occurred over almost entire EEC (Nikishin *et al.* 1996; Wilson & Lyashkevich 1996; Stephenson *et al.* 2006). These processes are evidenced to a large extent by the location of the deep source of rifting, as well as by the features of the lithotectonic complexes of the basement and composition of the Sarmatia crust. The seismic survey performed along the GR'13 profile runs along the strike of two major segments of the PDDB rift system: the PT and the DG, together with the DF—the southeastern inverted segment, which is crossed by the DOBRE'99 profile (WARR and CDP studies; DOBREfraction'99 Working Group 2003; Maystrenko *et al.* 2003). Obtained GR'13 seismic velocity model gave us valuable constraints for better understanding of the evolution of the Late Palaeozoic rift system of PDDB as a whole, including its individual segments corresponding to different phases of intracratonic rifting at the southern margin of the EEC.

6.1 Pripyat Trough

The western part of the GR'13 profile runs along the PT from NW to SE. The deposits of the PT overlap the OMIB—a wide belt of NE–SW strike, which is considered by Bogdanova *et al.* (1996) as a suture zone between Sarmatia and Fennoscandia (Fig. 2). The crust of the OMIB, with its large batholiths of gabbro-granodiorite-granite composition of 2.0–1.95 Ga, is characterized by a layered structure as the result of magmatic processes, collision, and post-collisional deformations (Bogdanova *et. al.* 2006).

According to the structure of the sedimentary cover of the PT and the velocity model of the consolidated crust of the OMIB, several main blocks can be identified in the uppermost crust along the GR'13 profile. Their boundaries relate with known faults and fault zones, which correlate with the relief of the basement (Fig. 3). Deeper, in the upper-middle crust, it is hard to trace the blocks boundaries due to lack of horizontal velocity contrasts (Fig. 6). In the lower crust and upper mantle, some features may suggest differences between blocks. According to the CDP studies on the VIII profile in the PT (Juhlin *et al.* 1996), the faults in the consolidated crust under the PT are flattened out at the top of the reflective lower crust, not penetrating deeper and not reaching the Moho.

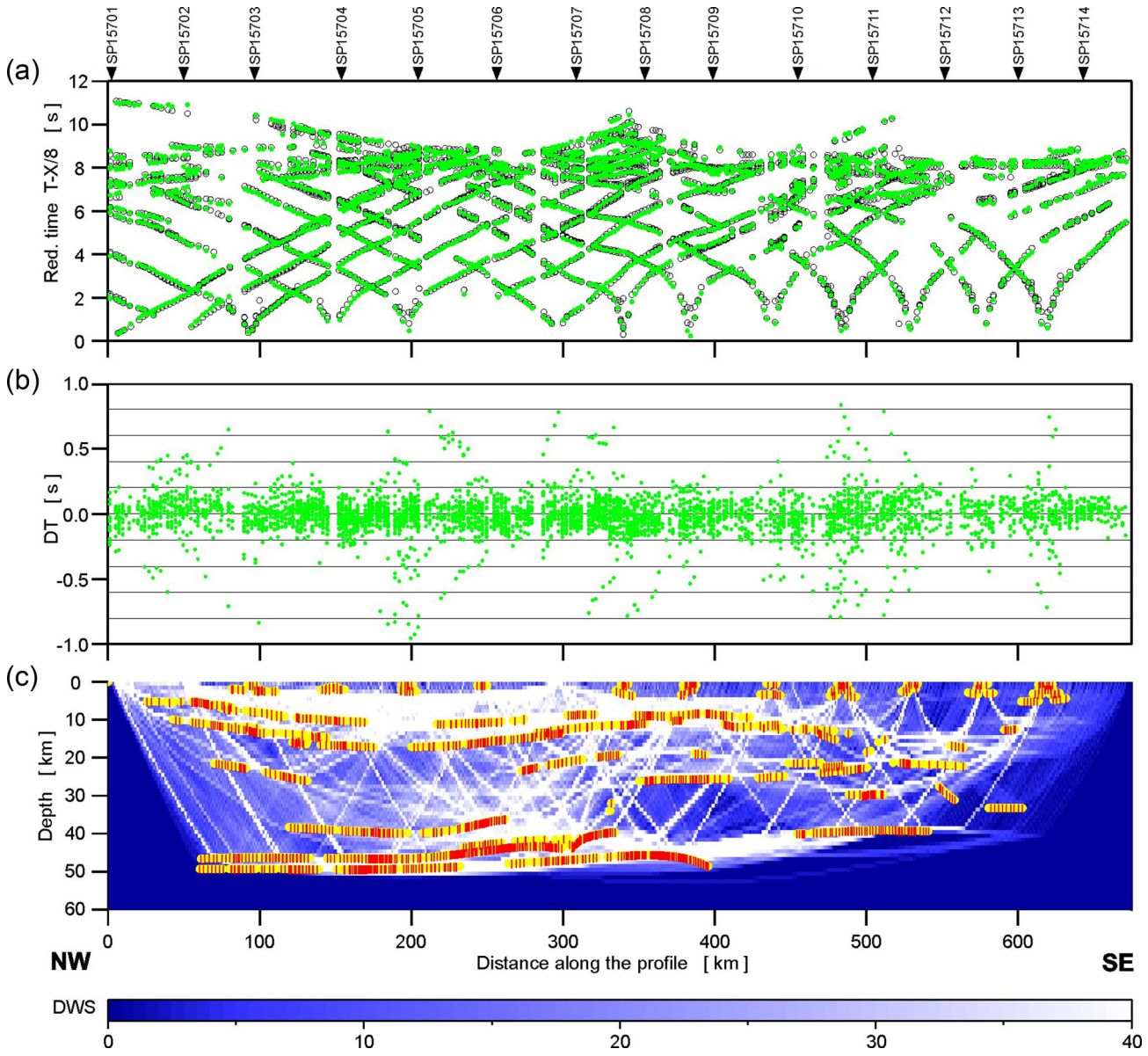

Figure 9. Diagrams showing theoretical and observed traveltimes (a), traveltime residuals (b) and ray coverage (c) from forward modelling along the profile. Green points: *P*-wave arrivals; black circles: theoretical traveltimes. Yellow lines: fragments of discontinuities constrained by reflected phases. The red points plotted along the interfaces mark the bottoming points of the modelled reflected phases (every third point is plotted) and their density is a measure of the positioning accuracy of the reflectors. DWS: derivative weight sum. Reduction velocity is 8 km s^{-1}.

The GR'13 profile begins at the southernmost block of the Central Belarus Suture Zone, which is overlain by the Belarusian Anteclise (~SP15701–SP15702), separated by the fault (~ 60 km) from the PT (or rather its Chervonosloboda-Malodushin Threshold displayed on the geological cross-section in Fig. 3). In the central part of the PT, the Azeretsk-Khobdinsk Threshold (140—250 km) is separated from the BU by a fault zone of the Khoynik Uplift (270 km) (Fig. 3).

In general, the depth of seismic boundaries in the upper and middle crust of the OMIB increases by up to 7 km in the central part of the belt (overlapped by the sediments of the Azeretsk-Khobdinsk Threshold of the PT (Fig. 3), conformally with the increase in sedimentary layer thickness in the PT. Here it is worth to make a comparison with two recent WARR profiles—EUROBRIDGE'95&'96 (EB'95 &'96) and EUROBRIDGE'97 (EB'97) (EUROBRIDGE Seismic Working Group 1999; Thybo *et al.* 2003), which were crossed by the GR'13 profile (Figs 1 and 10). The NW end of the GR'13 profile just touches the EB'95 &'96 transect. Therefore, it is possible to compare the structure to the depth of ~10 km, where a layer with relatively high velocities, Vp > 6.6 km s^{-1}, were found along both profiles. Intersection with the EB'97 is located close to SP15704 of GR'13 in the centre of the PT. Sedimentary layers with similar thicknesses and velocities were found along both profiles. The upper crustal layers, with Vp ~ 6.25 km s^{-1} and Vp > 6.35 km s^{-1}, also show similar thicknesses. Two middle crustal layers, of about 23 km thickness and with Vp = 6.55–6.6 km s^{-1} and Vp = 6.85–6.95 km s^{-1} on the GR'13 profile, correspond to a single 19 km thick layer with Vp = 6.65–6.8 km s^{-1} in the EB'97 model (Fig. 10).

The composition of the upper and middle crust of the OMIB, determined by seismogravimetric modelling of EB'96 and EB'97 profiles (Kozlovskaya *et al.* 2001, 2004; Yegorova *et al.* 2004b),

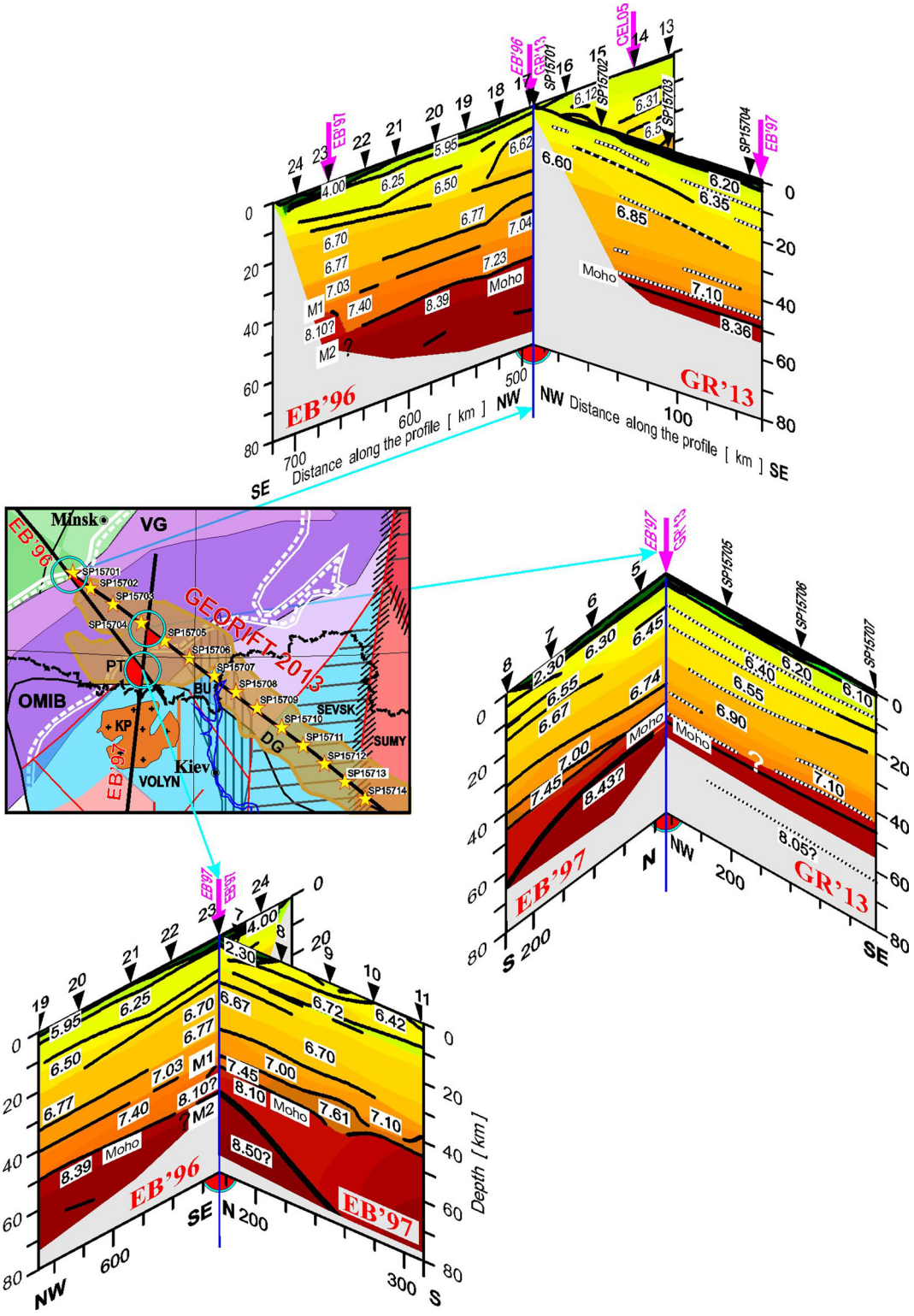

Figure 10. The intersection of the GEORIFT 2013 profile with EB'97 (Thybo *et al.* 2003) and EB'96 (EUROBRIDGE Seismic Working Group 1999) profiles. The crossing points of the three profiles in each point: EB'96/ GR'13, EB'97/ GR'13 and EB'97/EB'96. The model for the EB'96 profile has been reinterpreted and modified (Janik *et al.,* personal communication, 2009) with respect to original model (EUROBRIDGE Seismic Working Group 1999).

corresponds to magmatic rocks, varying with depth from granites to granodiorites and diorites. The deeper layer, according to velocities (6.8–7.0 km s^{-1}) and to composition of xenoliths from Devonian dikes (Markwick *et al.* 2001), may be represented by mafic granulites and, in part, by eclogite-like garnet-bearing granulites.

The top of the lower crust with Vp ~ 7.1 km s^{-1} was detected on the GR'13 profile at the depth of 40 km (Fig. 10), that is comparable with 37 km depth for the EB'97. Difference in depths of the Moho discontinuity is similar—it was modelled at 46 km along GR'13 and 43 km along EB'97. Also velocities in the uppermost mantle

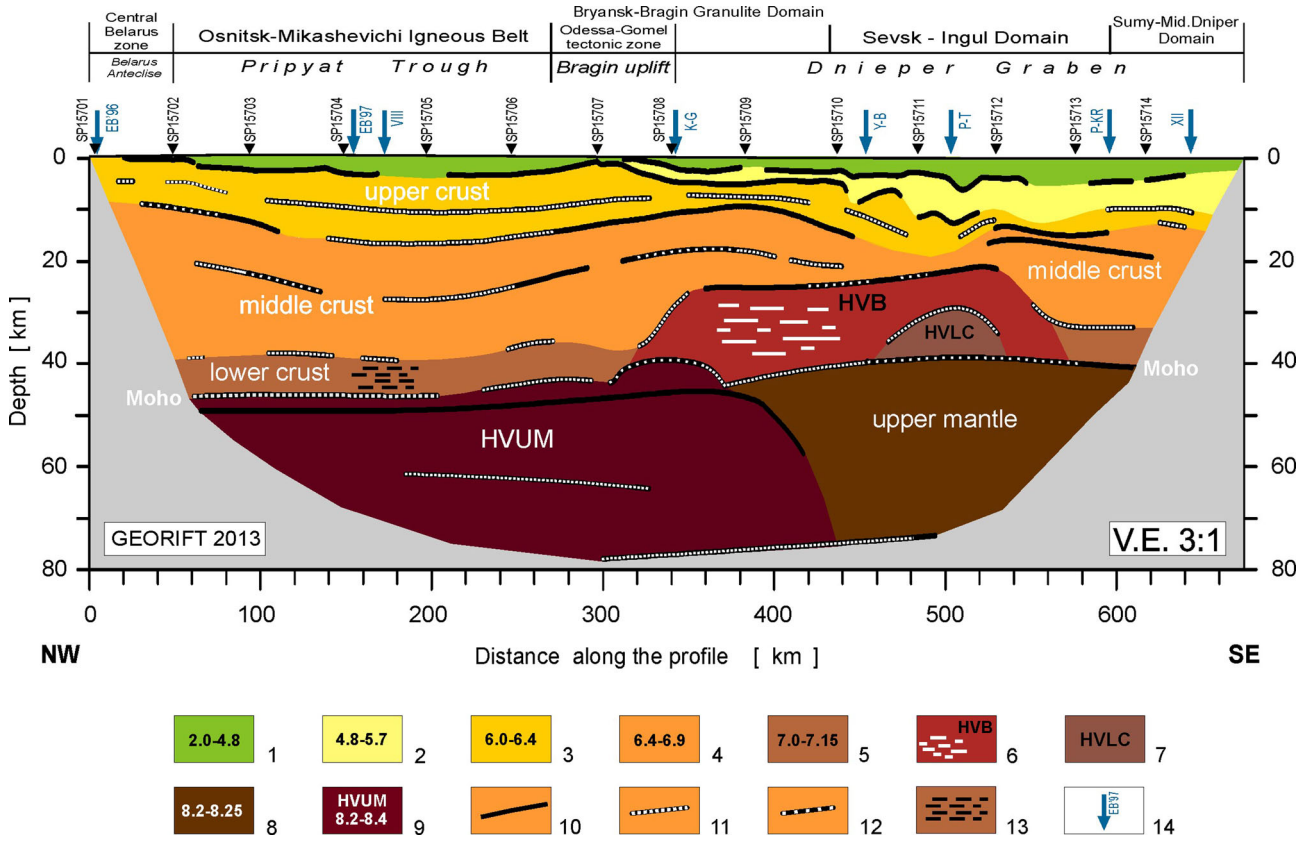

Figure 11. Simplified sketch of the lithospheric structure derived along the GEORIFT 2013 profile. (1) sedimentary cover (Vp = 2.0–4.8 km s^{-1}); (2) compacted sediments (Vp = 4.8–5.7 km s^{-1}); (3) crystalline uppermost crust (6.0–6.4 km s^{-1}); (4) middle crust (6.4–6.9 km s^{-1}); (5) lower crust (7.0–7.1 km s^{-1}); (6) high-velocity body; (7) high-velocity lower crust (7.35 km s^{-1}); (8) upper mantle (8.2–8.25 km s^{-1}); (9) high velocity upper mantle (8.2–8.4 km s^{-1}); (10–12) fragments of major boundaries interpreted from *P*-wave refractions, refractions and reflections, and reflections, respectively; (13) zones of high reflectivity in the lower crust from CDP profile VIII (Juhlin *et al.* 1996); (14) intersection points with other profiles. Shot point locations are shown by triangles above the profile.

for both models are somewhat different, Vp = 8.25 km s^{-1} and 8.1 km s^{-1}, respectively. In both models, a few km under the Moho discontinuity, zones with Vp > 8.35 km s^{-1} were found at depths 48 and 50 km, respectively. The zone of high velocities was proposed in the GR'13 model to explain traveltimes with high apparent velocity on the seismic sections SP15701–SP15705.

Complicated structure of the transition from the lower crust to the uppermost mantle (the Moho zone), distinguished below the central part of the PT, where the GR'13 is crossed by the EB'96 and EB'97 profiles in form of triangle (Fig. 1), and is shown in more detail in Fig. 10. Due to substantial differences in the interpretation of the lower crustal structure and in Moho depths for both EB profiles, the model for the southern end of the EB'96 was reinterpreted by T. Janik *et al*. (personal communication, 2009; Fig. 10). Velocities in lower crust and depths to the Moho in this case correspond much better to those modelled on the EB'97 (Thybo *et al.* 2003) at the intersection place, which is around 55 km from SP15705 on the GR'13.

We consider the PT origin according to a model of passive rifting associated with the formation of a shallow subhorizontal shear zone in the upper-middle crust (reflectors found along the (GR'13 and EB'96 profiles), and subsequent formation of the detachment zone through the whole crust. Common interpretation of WARR seismic data on the profile EB'97 and CDP data on the VIII profile in the PT (Juhlin *et al.* 1996) made it possible to trace the projection of such detachment in the upper mantle as a zone of increased stratification dipping SSE under the Ukrainian Shield (Aizberg & Starchik 2013).

The formation of the PT at the passive stage of rifting is consistent with the absence of a Moho uplift and a relatively large thickness of the crystalline crust (up to 46–48 km), as well as with the moderate *P*-wave velocity in the lower crust, which suggests that crust has not been reworked by Devonian rifting to the same degree as in the DG (Fig. 11). Thin high-velocity layer above the Moho in the PT could be the wedge of thick high-velocity body in the DG related to less pronounced rifting processes in the PT.

A commonly invoked scheme for the formation of the PT is the basin opening associated with a counter-clockwise rotation of a large crustal block in the area of BU (Chekunov 1976; Aizberg & Starchik 2013; Aizberg 2016).

Thus, the PT formed at the early stage of rifting as the closing link of the PDDB rift system with the critical role of extensional deformations along listric faults that control the flat (10°–20°) crustal detachment, and seem to propagate down to the upper mantle.

6.2 Dnieper Graben

The eastern part of the GR'13 profile runs along the main part of the DG (km 330–670), where thickness of sediments increases from ~1.7 km at the BU, separating the PT from the DG, to 12 km at the eastern end of the profile. According to the structure of the upper part of the model (sedimentary strata, basement and upper

crystalline crust), it is possible to distinguish three main blocks separated by faults.

The first, western, block, located in the NW part of the DG (SP15708–SP15710), includes the Skorinetskaya Depression and Nizhyn Trough (Fig. 3), filled with gently sloping syn- and post-rift sediments with Vp ranging from 2.28 to 5.0 km s^{-1} and average thickness of ~5 km (Fig. 6). This part of the rift overlies, most likely, the basement of Bragin massif, which is part of the Bryansk-Bragin granulite belt of the Paleoproterozoic age. In the upper/middle part of the crust, seismic boundaries with velocities of 6.4/6.6 km s^{-1} and 6.6/6.8 km s^{-1} are uplifted to depths of 10 and ~19 km, respectively, forming a wide arch (Figs 6 and 11).

The boundary between the first and the second blocks of the DG on the GR'13 profile could be tentatively traced near the SP15710, between the Bryansk-Bragin and the Sevsk-Ingul blocks of Sarmatia (Fig. 2). The thickness of the sediments in the second block, which fill the Sribnenska Depression and North-Yarov Trough, increases southeastwards, from 5 to 7.5 km mainly due to thicknening of the Carboniferous deposits (Fig. 3). These sediments cover in this part of the DG the crystalline basement of the Sevsk-Ingul block composed of 2.2–2.0 Ga Palaeoproterozoic granitoid rocks, with velocity of 6.2–6.25 km s^{-1} (Fig. 6). At the 15–19 km depth, the velocity dramatically increases to 6.6–6.7 km s^{-1}, suggesting more basic composition.

The eastern boundary of this block is, most likely, located between SP15713 and SP15714 and corresponds to the Ingulets-Krivoy Rog zone (the northern extension of the Krivoy Rog fault zone) that separates Sevsk-Ingul and Sumy-Middle Dnieper blocks of Sarmatia (Fig. 2). The Sumy-Middle Dnieper block (km ~590–670) is overlain by sediments of Sulimov Uplift and Landaryiska Depression (Fig. 3) with velocity increase from 2.4 km s^{-1} at the surface to 5.7 km s^{-1} at the bottom (12–13 km depth) (Fig. 6). The Carboniferous sediments with velocities of 5.2–5.7 km s^{-1} comprise the major part of the section at the depth range from 4–5 to 13 km (Figs 3 and 6). The Sumy-Middle Dnieper block, located at the SE end of the GR'13 profile, has thin (7–8 km) upper crust (Vp = 6.2–6.6 km s^{-1}) with the basement represented by Archean (3.2–2.8 Ga) rocks. These rocks, exposed at the Ukrainian Shield as large, irregular elongated greenstone belts that form a partition between voluminous domes of granite-gneisses (Shchipansky & Bogdanova 1996). Thick seismic layer with Vp = 6.75–6.88 km s^{-1} at the depth of 18–34 km is represented, most likely, by mafic granulites.

Distinctive feature of the DG is the high-velocity body (HVB) in the lower crust, which begins in the area of the BU and extends over a distance of 230 km (between 320 and 550 km) as 18–20 km thick body with velocity >7.1 km s^{-1}. Its top rises from 26 km at 300 km to 22 km at 530 km, and its base is located at the Moho—at the depth of 38–40 km in this part of the profile. In general, the velocity distribution within the HVB is quite homogeneous—the velocity increases from 7.10 km s^{-1} in the upper part of the body to ~7.17 km s^{-1} above the Moho, although the area of higher velocities (HVLC, Vp up to 7.30 km s^{-1}) is modelled in the lowest crust inside the HVB at 460–540 km distance (Figs 6 and 11).

Bodies of that type have been found in several rifts and are attributed to a 'rift pillow' or mantle underplate (Erving & McGinnis 1975; Behrendt *et al.* 1990; Keller & Baldridge 1995; Thybo *et al.* 2000; Keller & Stephenson 2007; Yegorova *et al.* 2011). This is a distinctive feature of the DG revealed by DSS and gravity modelling (Ilchenko 1996; DOBREfraction'99 Working Group 2003; Starostenko *et al.* 1986; Yegorova *et al.* 1999, 2004a, Kozlovskaya *et al.* 2004). It is interpreted as a high-velocity and high-density crustal body in the DG, indicative of extensive magmatic underplating during rifting. This process also led to substantial modification of the uppermost mantle and to a Moho uplift below the axial part of the basin in comparison with the rift shoulders in the area of the Voronezh Massif and Ukrainian Shield, with Moho depths of 40–45 km (Sollogub 1986). This uplift is even larger if compared with the Moho at 46–50 km depth below the PT (Fig. 6).

The HVB has rather large extent (between SP15708 and SP15712-SP15713), though it is not distinguished along the whole DG as a single high-velocity body. Southeast of 550 km distance, the HVB dramatically thins to 7–8 km and is overlaid by a ~13 km thick layer with velocity of 6.8–6.88 km s^{-1} (Fig. 6). Such velocity structure of the lower crust is very similar to the region located to the NW of the DG—below the BU and the PT. It is noteworthy to say that the HVB in the DG along the GR'13 correlate well with two major gravity anomalies—the Chernigov and Lohvyts highs of 80 and 40 mGal amplitude correspondingly (Fig. 6). These gravity highs are explained mainly by high-density mantle rocks (density of ≥3.0 g cm^{-3}) of mafic/ultramafic composition intruded into the lower crust during rifting, which form the rift pillow or 'axial dyke' of the DG (Starostenko *et al.* 1986; Yegorova *et al.* 1999, 2004a).

Seismic model (Fig. 6) and its interpretation (Fig. 11) indicate heterogeneous inner structure of the HVB—its NW part is characterized by strong reflectivity, while in the SE portion a body with higher velocities (up to 7.30 km s^{-1}) has been distinguished. Reflective HVB has been indicated in the Donbas segment (DF) of the PDDB from recent studies on the lower crustal reflectivity (Lyngsie *et al.* 2007; Carpentier *et al.* 2009). They have shown that the HVB includes a series of high-velocity layers with individual thickness of the order 400–700 m and strong seismic velocity contrast (Lyngsie *et al.* 2007). They are interpreted as a mantle melts intruded as sills and dykes into the lower crust during late Devonian rifting.

The DG part of the GR'13 is intersected on the territory of Ukraine by the DSS lines acquired in 60–80th of last century. Figs 1 and 2 show location of some of them: four lines crossing the rift profiles—Kiev-Gomel (Kalyuzhnaya & Ryabchun 1985; Sollogub 1986), Yagotyn–Baturin (Y-B; Baranova & Kozlenko 1989), Piryatyn–Talalaivka (P-T; Ilchenko 1996), Putyvl-Krivoy Rog (P-KR; Chekunov *et al.* 1992b) and the geotraverse XII (Poltava–Sverdlovsk; Sollogub 1986) that runs along the strike of the rift and starts near the SE end of the GR'13 profile. Generally, they were measured and interpreted by using the methodology of that time, with analogue recordings on photo paper and mainly by 1-D modelling of first arrivals. Later, in the 90-ties, some profiles were reinterpreted using the programs applying solution of direct kinematic problem (Baranova & Kozlenko 1989; Ilchenko 1996). Therefore, a comparison of the structures at the intersections with these models must be done with caution, keeping this aspect in mind.

The GR'13 is crossed by the DSS profile Kiev-Gomel (Kalyuzhnaya & Ryabchun 1985; Sollogub 1986) near the SP15708 in the region of highest gravity anomaly—the Chernigov maximum (Figs 2 and 6). Velocity model on the GR'13 profile is in good agreement with the Kiev-Gomel seismic model, as regards 5-km thick sediments, structure of the upper and middle crust (Vp = 6.1–6.6 km s^{-1}) down to the depth of ~20 km; high-velocity lower crust is found on both profiles at ~30 km depth. The model for Yagotin-Baturin profile documents structure of the crystalline crust only, with comparable thickness of sediments in the area of intersection with GR'13 profile. The model of the profile Piryatin-Talalaevka, prepared by 2-D forward modelling, seems to be of better quality. It crosses the GR'13 at area where a thick (~17 km) HVLC with

Vp = 7.1–7.3 km s^{-1} is observed. Similar depths of the both the HVLC and the Moho boundary (∼38 km) are observed on both profiles. The Putyvl-Krivoy Rog and XII profiles show very similar structures at the intersections with the GR'13 concerning the thickness of the crustal layers, the *P*-wave velocities and depths to the Moho (∼38 and ∼40 km respectively).

In the GR'13 model there is also a large difference in velocities below the Moho—compared to high velocities (8.36 km s^{-1}) under the PT, velocities of 8.20–8.25 km s^{-1} below the DG can suggest substantial upper mantle modification due to rifting, which affected mainly the DG (Fig. 11). Low-velocity mantle is characteristic for many rift zones, and is interpreted to be caused by partial melting (3–5 percent) of basaltic magma rising from greater depth (base of lithosphere) up to the Moho (Makris & Ginzburg 1987; Prodehl *et al.* 1992; Achauer *et al.* 1994).

Comparison of the Moho depths and velocities along the GR'13 profile with previously acquired DSS lines shows that the only significant difference concerns the *P*-wave velocity in the uppermost mantle. Along the profiles Putyvl-Krivoy Rog and XII it was modelled as 7.8–7.9 km s^{-1}, while on the GR'13 it is higher and amounts to ∼8.2 km s^{-1}. This may be due to the relatively short branches of the Pn phase recorded in old seismic sections and additionally because of older modelling technique (the method of effective parameters) used in past years for modelling of the reflected phases (e.g. Egorkin 1966; Grad 1983). For the WARR data, the value of the effective velocity may exceed the value of the mean velocity even by 10–15%. Another important feature observed on the profile Putyvl-Krivoy Rog, just south of the intersection, is a significant (∼10 km) increase in the depth of the Moho boundary, to a depth of ∼50 km. This may be the origin of several strong reflections that are observed in seismic sections of the SE end of the profile GR'13, and which do not lend themselves to common modelling with most of reflected traveltime branches accepted during correlation and modelling as consistent and representative for a 2-D model.

6.3 BU of the basement (junction area between PT and DB)

The tectonic position of the BU separating the PT and DG is associated with the Proterozoic faults of the NS and NE strike (Chekunov 1994; Aizberg & Starchik 2013; Aizberg 2016), at the intersection of which the change in the strike of the PDDB rift zone occurs. BU (270–330 km distance) became the centre of the hinge fracture of the PDDB (Fig. 2).

BU is characterized by the elevation of the basement to 1.5 km, which is represented by the Paleoproterozoic rocks of the Bryansk-Bragin granulite belt (Fig. 2; Bogdanova *et al.* 2006). The junction area between the PT and the DG coincides with the area of considerable magmatic activity, evidenced by Upper Devonian alkaline-basalts and alkaline-ultrabasic rocks and their differentiates, reaching 3 km thickness. The age of volcanogenic formations (Late Frasnian–Famennian) and of related intrusive magmatism corresponds to the main phase of active rifting (Wilson & Lyashkevich 1996).

Late Devonian magmatic activity led to modification of the crust and the upper mantle structure observed in the velocity model of the GR'13 profile in the area of the BU. Here the sub-Moho velocity below the PT is ∼8.2 km s^{-1}, while deeper, the second upper mantle boundary with 8.35 km s^{-1} dips from ∼45 to ∼55 km at distances of 370—420 km—just at the place of its contact with the upper mantle of the DG with Vp = 8.25 km s^{-1} (Fig. 6). That, together with the ∼4 km deflection of the Moho, forms an anomalous contact zone in the Moho-uppermost mantle region. Also, in this place, the high-velocity body HVLC of the DG begins. It should be noted that uppermost mantle seismic discontinuity beneath the Moho with velocity of 8.35 km s^{-1} correlates well with a reflector revealed on the NS profile EB'97 in the upper mantle, which dips in SSE direction beneath the Ukrainian Shield (Fig. 10).

The junction zone of the PT and the DG in the region of the BU is located at the node of its intersection with the faults of the NE strike that bound the southern edge of the OMIB and with the NS-trending Odessa-Gomel tectonic zone (Fig. 2). The tectonic zone Odessa-Gomel, being a part of large zone extending through the whole continent from the Black Sea to the Barents Sea (Bogdanova 1984; Dedeev & Nalivkin 1994), played a role in regional tectonics of the study area (Yegorova *et al.* 2004b; Starostenko & Stephenson 2006; Aizberg & Starchik 2013). Our interpretation of the lower crust structure on the GR'13 profile (Fig. 11) confirms an important role of this zone, which was, most likely, a barrier to the propagation of the rifting processes to the NW direction; therefore, the processes of active rifting affected mainly the DG.

6.4 Donbas Foldbelt

The DF, representing the closing segment of the PDDB rift zone, affected by post-rift activation and partial inversion, was not reached by the GR'13 profile, but it is well studied by recent seismic experiment along the DOBRE'99 profile, including the WARR and deep CDP studies (DOBREfraction'99 Working Group 2003; Maystrenko *et al.* 2003). To obtain a more complete picture of the structure of the whole PDDB rift zone, we briefly describe it here according to DOBREfraction'99 Working Group (2003) and Maystrenko *et al.* (2003).

Very deep Palaeozoic graben of the DF is filled with metasedimentary rocks of the Carboniferous age with Vp = 5.2–5.8 km s^{-1} and thickness > 20 km. The folded Carboniferous complex is exposed on the surface and forms a well-known coal basin. The Devonian magmatism of the DF is very similar to that of the DG. Interpretation of seismic data on the DOBRE'99 profile has shown the similarity of the deep structure of DF and DG—namely, the same depths to the Moho (38–40 km) and the presence of the HVLC body with Vp = 6.8–7.2 km s^{-1} (of asymmetric shape in the DF) at approximately the same depths.

Inversion structure of the DF was observed on the CDP cross-section DOBRE'99 as a rather simple model of continental rifting of the mega pop-up structure with two bounded faults of opposite dips; the main listric fault of the southern dip, traced from the surface in the northern thrust zone to the Moho (Maystrenko *et al.* 2003). This pop-up structure was elevated along the main listric fault and moved northwards on the Voronezh Massif due to compressional deformations directed from the south. As a result of the uplift, estimated to be up to 6 km (Stovba & Stephenson 1999), the Carboniferous deposits were brought to the surface. The main phase of compressional deformations, responsible for a partial inversion of the DF, according to the new studies (Stovba & Stephenson 1999; Saintot *et al.* 2003) is dated to the Cretaceous-Paleogene boundary (Alpine deformations)—contrary to traditional view that the inversion occurred in the DF in the early Permian, simultaneously with the Uralian orogeny.

6.5 Tectonic evolution of the PDDB

A peculiar horizontal shape of the PDDB resembles the stretched 'Z' configuration with notable change in the strike of three main

segments in the area of the BU of the basement, separating the PT and the DG, and the similar saddle between the DG and DF. This may indicate that in the initial phase of rifting (from Early to Late Frasnian), occurred in the environment of dextral strike-slip along the Sarmato-Turanian lineament, the PT and DG developed in the regime of passive rifting (Aizberg & Starchik 2013; Aizberg 2016).

Segmentation of the PDDB into three main segments could be associated with main phases of continental rifting—from passive rifting in the PT to its active phase in the DG—followed by basin inversion in the DF segment. Such segmentation of the PDDB is in good agreement with the idea of Chekunov (1994) about increasing of rifting activity in the SE direction—from the PT to the DF and is in good correspondence with the velocity model on the GR'13 profile.

The PDDB evolved during the Middle and the Late Devonian by northwestward rift propagation from the Peri-Caspian Basin area (Gavrish 1989; Nikishin *et al.* 1996; Wilson & Lyashkevich 1996). The sedimentary fill of the PDDB decreases in thickness from ∼20 km in the DF to about 2.5 km in the PT in accordance with the rift width and magnitude of crust stretching (Gavrish 1989; Chekunov *et al.* 1992a; Stephenson *et al.* 1993; Kusznir *et al.* 1996a,b; Stovba *et al.* 1996; van Wees *et al.* 1996).

The passive rifting regime in the PDDB was changed in the Late Famennian–Frasnian time by the active rifting in the DG and DF (Donbass) due to ascent of plumes from the depths of lithosphere base. Conventionally, this time is regarded (by many scientists) as the main phase of active rifting, the most evident and the best studied in the DG. It is characterized by a significant magmatism, increase in velocity and amplitude of immersion of blocks, uplift of the Moho along the central part of the DG, occurrence of the deflection of the Moho, the reflector dipping into the upper mantle (at the junction of the PT and DG) and formation of the rift pillow under the DG (Fig. 11; Gavrish 1989; Lukin 1997; Chekunov 1994; Nikishin *et al.* 1996; Wilson & Lyashkevich 1996; Stephenson *et al.* 2006). The rift pillow, associated often with the Moho uplift and low-velocity zone below the Moho, is a distinctive feature of many rift zones and is clearly seen in the velocity model on the GR'13 profile (Figs 6 and 11). It shows that the rift pillow in the DG of ∼230 km size has rather heterogeneous lateral structure with more reflective and laminated part in the NW part and an occurrence of higher velocities (to 7.3 km s^{-1}) in its SE part. The rift pillow is underlain by the Moho uplift with the sub-Moho velocities decreasing to 8.20–8.25 km s^{-1} in comparison to 8.35 km s^{-1} below the PT.

One of the plumes, regarded as a possible mantle sources for the DG rifting, could be located below the Peri-Caspian Basin (Chekunov 1994). Gravity modelling has shown that residual gravity anomalies above the DG-DF and the Peri-Caspian Basin, caused by a high-density material in the lower crust associated with HVLC, are interpreted in terms of two branches of the same Middle-Late Devonian rift system with the locus in the Peri-Caspian Basin area (Yegorova *et al.* 2004a). Stephenson *et al.* (2006) concluded that the PDDB in the SE opened into a deep basin, possibly having oceanic lithospheric affinity, in the area where it adjoins the southern Peri-Caspian Basin (the area of possible triple junction of rifts), suggesting that rifting led to limited continental break-up in this part of southeastern margin of the EEC at this time.

Within the southern margin of the EEC, this could be not one plume, rather a cluster of several plumes or geochemical-thermal instabilities. Another such centre could be located in the area of the NW part of the DG and BU, which is associated with considerable Late Devonian magmatic activity and crustal underplating seen in the velocity model on the GR'13 as thick HVLC body (Fig. 6). Lithospheric sources of such paleo-plumes could be seen from seismic noise surface-wave tomography of the East European Platform (Koroleva *et al.* 2010). A low-velocity zone, revealed at the depth of 200–300 km below the NW part of the DG, could be a relict of a plume-like structure. Another similar structure was detected at 100–220 km depth below the Peri-Caspian Basin (Koroleva *et al.* 2010). It is difficult to say with certainty about the formation mechanism of these low-velocity upper mantle domains in regards to the crustal underplate (rift pillow) in the DG, but their areal relationship is evident, especially taking into account that they coincide with both areas of strong gravity anomalies and considerable Late Devonian magmatic activity. In addition, this part of the rift pillow (∼km 340–440) is characterized by considerable seismic reflectivity, which suggests existence of thin higher and lower velocity layers, caused by layered intrusions of mantle melt. Some evidence of such phenomena is presented by Lyngsie *et al.* (2007) in their study of lower crust reflectivity in the DF segment of the PDDB.

With its NW direction, the rift separates the Sarmathian Shield into two parts—the Ukrainian Shield in the south and the Voronezh Massif in the north, both characterized by common Archean-Paleoproterozoic lithotectonic provinces separated by the Late Proterozoic suture zones (Shchipansky & Bogdanova 1996; Fig. 2). Therefore, the peculiarities of rifting in three segments of the PDDB, as well as the related structure of the rift basin and reworked crust could be determined to a certain extent by the features of these Precambrian domains and basement blocks of different composition separated by fault zones. It is known that boundaries of the main segments occur at the intersections of the rift with the NS-oriented Late Proterozoic faults. In such a 'node' of crossing fault zones the BU is located, separating the PT of general WE strike from the NW-oriented the DG (Fig. 2). A similar situation is also observed at the transition of the DG to the DF.

Earlier origin of rifting in the SE of the PDDB, propagating northwestwards, corresponds with the thickness of sediments (syn-rift and post-rift sediments) that decrease from >20 km in the DF to >10 km in the DG and 5–6 km in the PT. In accordance with these, the 'stretching factors' are estimated as 2.25–2.5, 1.3 and ∼1.1 for the DF, DG and PT respectively (Kusznir *et al.* 1996a,b; DOBREfraction'99 Working Group 2003). The seismic studies, performed on the GR'13 profile and on the EB'96 (Eurobridge Seismic Working Group 1999) and the EB'97 (Thybo *et al.* 2003) in the PT, as well as on the DOBRE'99 profile (DOBREfraction'99 Working Group 2003) in the DF, have shown that the amount of crystalline crust thinning beneath the PDDB also increases to the SE in accordance with increasing sedimentary thickness—from 42–45 km below the PT to ∼30 km and >20 km in the DG and DF, correspondingly.

A distinctive trace of the Late-Middle Devonian rifting in the PDDB is the ∼17 km thick high-velocity (HVLC) and high-density body related to crustal underplate or 'rift pillow', which extends below the major part of the DG with a length of 230 km (SP15708–SP15713). In the DF, the HVLC thickens to 20 km (DOBREfraction'99 Working Group 2003).

Thus, several evidences for active rifting in Late-Middle Devonian: from the structure of the sedimentary cover, magmatism, stretching factors, to the structure of the crust with the presence of the HVLC, the Moho relief and velocities under the Moho, were manifested in the DG. The lack of the Moho uplift and the large thickness of the crust under the PT (up to 46–48 km) is explained by position of the PT as the closing link of the PDDB with attenuation of rifting in the NW direction. The crust here was not reworked by Late-Middle Devonian rifting as strongly as it was in the DG.

A special role is played by the BU located within the NS tectonic zone Odessa-Gomel, which 'blocked' the northward propagation of active rifting into the PT.

The close location of the DF segment to the southeastern boundary of the craton (EEC) probably predetermined its further post-rift activation and tectonic inversion. The peak of these processes is caused by Alpine compressional deformations that led to the formation of a 'mega pop-up' type crustal structure and bringing to the surface coal deposits of Carboniferous age (Stovba & Stephenson 1999; Saintot *et al.* 2003).

7 CONCLUSIONS

New WARR seismic studies on the GR'13 profile, performed along the Late Palaeozoic intracratonic rift system of the PDDB, provide new constraints for study of basin architecture and structure of the crust and uppermost mantle of two major segments of the PDDB rift and help to understand better the processes of intracratonic rifting on the southern margin of the EEC.

The two major segments—the PT and the DG—are characterized by different structure of the crust and upper mantle caused by varying intensity of rifting in the PDDB and represent two phases of rifting—passive and active. The PT was formed in the initial rifting stage in the environment of ∼NS extension along a system of listric faults controlling the detachment in the crust and upper mantle.

The absence of the Moho uplift and relatively large crystalline crust thickness under the PT is explained by the tectonic position of the PT as a closing unit of the PDDB, with a gradual attenuation of rifting from the southeast to the northwest. Here, the crust represented by rocks of OMIB was not reworked as strongly by Late Devonian rifting as in the DG segment. The PT evolved as a passive rift up to the final rifting stage in the Middle Carboniferous time.

Active stage of rifting (Late Frasnian–Late Famennian time), following the passive phase, is evidenced in the DG by a shallower Moho (in comparison with the PT) along the central part of the graben, and by a presence of an HVLC, known as rift pillow or mantle underplate. The HVLC in the DG, with velocities 7.10–7.17 km s^{-1} and ∼18–20 km thickness, extends for ∼230 km along the major part of the DG. It is caused by mantle intrusions of mafic and ultramafic composition during the active phase of rifting due to ascent of mantle plume. This associates with considerable volume of magmatism in the DG.

The junction zone of the PT and the DG in the area of BU of the basement can be observed as the division between the zones of passive and active rifting. This is clearly seen in Fig. 11 as a change in the structure of the crust and upper mantle—the appearance of inclined seismic boundary below the Moho at a depth of ∼50 km with *P*-wave velocity of 8.35 km s^{-1} (under the PT) and 8.20–8.25 km s^{-1} (below the DG). Together with a deflection of the Moho of ∼4 km- amplitude, it forms a single anomalous structure at the Moho–sub-Moho depths. In the lower crust, the PT/BG boundary can be traced at the edge of the HVLC body of the DG.

With the general trend of attenuation of rifting in the NW direction, there is a tendency for the transverse division of the PT and the DG in several segments (approximately) at the places of crossing the Archean-Paleoproterozoic lithotectonic provinces of Sarmatia (Ukrainian Shield and Voronezh Massif) by NS-oriented Late Proterozoic suture zones. This is especially evident in the BU, located at its intersection with the NS regional tectonic zone Odessa-Gomel. Most likely, the 'blocking' effect of this zone did not allow for further propagation in NW direction of active rifting within the PT. This has led, apparently, to the change in the amount of the extension of the rift zone and to deflection from its general NW orientation to the WE trend in the PT segment.

ACKNOWLEDGEMENTS

The GR'13 profile was acquired in international collaboration between institutions and organizations from Ukraine (Institute of Geophysics, National Academy of Sciences of Ukraine, and the State Geophysical Enterprise 'Ukrgeofizika', Kiev); Belarus (Institute for Nature Management of the National Academy of Sciences of Belarus, and State Enterprise 'NPC in geology'); Poland (Institute of Geophysics, Polish Academy of Sciences, Warsaw); Denmark (Geology Section, IGN, University of Copenhagen); Finland (Institute of Seismology, University of Helsinki). Participation of the Polish group at this work was supported within statutory activities No 3841/E-41/S/2017 of the Ministry of Science and Higher Education of Poland. The authors express their sincere appreciation of the activities by the many people who took part in field work and data acquisition. The authors are sincerely grateful to the 'Geophysical Journal International' editor prof. Gabi Laske and reviewers: prof. Randy Keller (University of Oklahoma, USA) for high opinion of our work and prof. Marek Grad (University of Warsaw, Poland) for helpful comments and suggestions.

REFERENCES

Achauer, U. & the KRISP Teleseismic Working Group, 1994. New ideas on the Kenya rift based on the inversion of the combined dataset of the 1985 and 1989/90 seismic tomography experiments, *Tectonophysics,* **236**(1–4), 305–329.

Aizberg, R.E., Garetskij, R.G. & Sinichka, A.M., 1971. Sarmatsko-Turanian lineament of the Earth's crust, in *Problems of Theoretical and Regional Tectonics*, ed. Peive, A.V., Nauka (in Russian).

Aizberg, R.Ye., 2016. About segmentation of the Pripyat-Dnieper-Donets aulakogen, *Dokl. Natl. Acad. Sci. Belarus,* **60** (6), 111–116 (in Russian).

Aizberg, R.Ye. & Starchik, T.A., 2013. *Synrift Geodynamics of the Pripyat Trough,* Belaruskaya navuka, pp. 146 (in Russian).

Aksamentova, N.V., 2002. *Magmatism and Paleogeodynamics of Early Proterozoic Osnitsk-Mikashevichi Volcanic-Plutonic Belt,* Minsk, pp. 176 (in Russian).

Aksamentova, N.V. & Naidenkov, I.V., 1990. *Geological Map of Crystalline Basement of Belarus and Adjoining Territories 1:100 000 Scale,* Minsk (in Russian).

Baranova, E.P. & & Kozlenko, V.G., 1989. Velocity model of the crust of the Dnieper Graben, *Geophys. J.,* **11**(5), 81–88 (in Russian).

Behrendt, J.C., Hutchinson, D.R., Lee, M., Thornber, C.R., Tréhu, A., Cannon, W. & Green, A., 1990. GLIMPCE Seismic reflection evidence of deep-crustal and upper-mantle intrusions and magmatic underplating associated with the Midcontinent Rift system of North America, *Tectonophysics,* **173**(1–4), 595–615.

Bogdanova, S. *et al.*, 2006. EUROBRIDGE: new insight into geodynamic evolution of the East European Craton, *Geol. Soc., London, Mem.*, **32,** 599–625.

Bogdanova, S.V., 1984. Tectonics of the basement of East European platform, in *Tectonic Investigation of the Western part of the East European Platform*, pp. 16–28, ed. Bogdanova, S.V., Nauka i Tehnika (in Russian).

Bogdanova, S.V., 1993. Segments of the East European Craton, in *EUROPROBE in Jablonna 1991*, pp. 33–38, eds Gee, D.G. & Beckholmen, M., Inst. Geophysics, Pol. Acad. Sci.

Bogdanova, S.V. & Garetsky, R.G., 2006. Project EUROBRIDGE: Paleozoic accretion and collision of the crust in Fennoscandia and Sarmatia, Geology and geophysical images, in *Structure and Dynamics of the Lithosphere of Eastern Europe*, *Results of the Research on the EUROPROBE Program*, pp. 223–290, ed. Bogdanova, S.V., GEOKART GEOS (in Russian).

Bogdanova, S.V., Pashkevich, I.K., Gorbatschev, R. & Orlyuk, M., 1996. Riphean rifting and major Palaeoproterozoic crustal boundaries in the basement of the East European Craton: geology and geophysics, *Tectonophysics,* **268**(1–4), 1–21.

Carpentier, S.F.A., Roy-Chowdhury, K., Stephenson, R.A. & Stovba, S., 2009. Delineating tectonic units beneath the Donbas Fold Belt using scale lengths estimated from DOBRE 2000/2001 deep reflection data, *J. geophys. Res.,* **114**(B10), B10315, doi:10.1029/2008JB006124.

Červený, V. & Pšenčík, I., 1984. SEIS83 - numerical modelling of seismic wave fields in 2-D laterally varying layered structures by the ray method, in *Documentation of Earthquake Algorithms*, pp. 36–40, ed. Engdahl, E.R., Rep. SE-35, World Data Cent. A for Solid Earth Geophysics, Boulder, Colo.

Chekunov, A.V., 1976. About moving apart and rotation of blocks of the Earth's crust in formation of the Dnieper-Donets aulakogen, *Geol. J.,* **1,** 123–127 (in Russian).

Chekunov, A.V., 1994. The geodynamics of the Dnieper-Donets Rift syncline, *Geophys. J.,* **16**(3), 3–13 (in Russian).

Chekunov, A.V., Gavrish, V.K., Kutas, R.I. & Rybchun, L.I. 1992a. Dnieper-Donets palaeorift, *Tectonophysics,* **208**(1–3), 257–272.

Chekunov, A.V., Kivshyk, N.K., Kharitonov, O.M., Omelchenko, V.D. & Tolkunov, A.P., 1992b. Profile Putyvl-Krivoi Rog through ultradeep wells of Ukraine, *Geophys. J.,* **14**(1), 3–10 (in Russian).

Chekunov, A.V., Kayuzhnaya, L.T. & Ryabchun, L.I., 1993. Deep structure and oil and gas bearing of the Dnieper-Donets paleorift, in *Rifting and Oil and Gas Bearing*, pp. 16–24, eds Khain, V.E., Sokolov, B.A. & Marasanova, N.V., Nauka (in Russian).

Chirvinskaya, M.V. & Sollogub, V.B., 1980. *Deep Structure of the Dnieper–Donets Aulacogen from Geophysical Data,* Naukova Dumka (in Russian).

Chirvinsky, V., 1928. About some effusive rocks of Volyn from the former Novogradvolyn and Zhytomir region and about the fault zone in the northwestern part of the Ukrainian Crystalline Belt, *Visnik Ukrainian Geol. Committee,* **11,** 187–209 (in Russian).

Dedeev, V.A. & Nalivkin, D.V. (eds), 1994. *Tectonic Map of the USSR Territory, 1:5 000 000 scale,* Academy of Sciences of the USSR, Institute of geochronology of Precambrian of AS USSR, Ministry of Geology of the USSR.

DOBREfraction'99 Working GroupGrad, M. *et al.*, 2003. "DOBREfraction'99"—velocity model of the crust and upper mantle beneath the Donbas Foldbelt (East Ukraine), *Tectonophysics,* **371**(1–4), 81–110.

Egorkin, A.V., 1966. Analysis of the accuracy determination of velocity cross-section in the Earth's crust from travel time of reflected waves, *Izv. Akad. Nauk SSSR, Fiz. Zemli,* **9,** 72–81 (in Russian).

Eisenverg, D.E. (ed), 1988. *Geology and Oil and Gas Occurrences of the Dnieper–Donets Depression: Stratigraphy,* Naukova Dumka (in Russian).

Ervin, C.P. & McGinnis, L.D., 1975. Reelfoot rift: reactivated precursor to the Mississippi Embayment, *Bull. geol. Soc. Am.,* **86**(9), 1287–1295.

EUROBRIDGE Seismic Working Group, 1999. Seismic velocity structure across the Fennoscandia–Sarmatia suture of the East European Craton beneath the EUROBRIDGE profile through Lithuania and Belarus, *Tectonophysics,* **314**(1–3), 193–217

Garetsky, R.G. (ed), 1979. *Tectonics of the Pripyat Trough*, pp. 222, Nauka i Technika, (in Russian).

Garetsky, R.G. & Klushin, S.V., 1989. Listric faults in the Pripyat Paleorift, *Geotectonics,* **23,** 36–44.

Gavrish, V.K. 1989. *Geology and Oil and Gas Potential of the Dnieper–Donets Depression: Depth Structure and Geotectonic Evolution,* Naukova Dumka (in Russian).

Gee, D.G. & Zeyen, H. (eds), 1996. *EUROPROBE 1996—Lithosphere Dynamics—Origin and Evolution of Continents*, pp. 138, EUROPROBE Secretariat, Uppsala University.

Grad, M., 1983. Determination of mean velocities and depths of boundaries in the Earth's crust from reflected waves, *Acta Geophys. Pol.,* **31,** 231–241.

Grad, M. *et al.*, 2003. DOBRE-99: The crust structure of the Donets Basin along the Mariupol-Belovodsk Profile, *Izv. Phys. Solid Earth,* **39,** 464–473.

Grad, M. *et al.*, 2006a. Lithospheric structure beneath trans-Carpathian transect from Precambrian platform to Pannonian basin: CELEBRATION 2000 seismic profile CEL05, *J. geophys. Res.,* **111**(B3), B03301, doi: 10.1029/2005JB003647.

Grad, M., Janik, T., Guterch, A., Środa, P. & Czuba, W. & EUROBRIDGE'96–97, POLONAISE'97 & CELEBRATION 2000 Seismic Working Groups, 2006b. Lithospheric structure of the western part of the East European Craton investigated by deep seismic profiles, *Geol. Q.,* **50**(1), 9–22.

Ilchenko, T.V., 1996. Dniepr-Donets Rift: deep structure and evolution from DSS profiling, *Tectonophysics,* **268**(1–4), 83–98.

Janik, T., Yliniemi, J., Grad, M., Thybo, H. & Tiira, T. & POLONAISE P2 Working Group, 2002. Crustal structure across the TESZ along POLONAISE'97 seismic profile P2 in NW Poland, *Tectonophysics,* **360**(1–4), 129–152.

Janik, T., Grad, M. & Guterch, A. & CELEBRATION 2000 Working Group, 2009. Seismic structure of the lithosphere between the East European Craton and the Carpathians from the net of CELEBRATION 2000 profiles in SE Poland, *Geol. Q.,* **53**(1), 141–158.

Juhlin, C., Stephenson, R.A. & Klushin, S., 1996. Reappraisal of deep seismic reflection profile VIII across the Pripyat Trough, *Tectonophysics,* **268**(1–4), 99–108.

Kalyuzhnaya, L.T. & Ryabchun, L.I., 1985. The structure of the deep horizons of the crust and sedimentary cover on the DSS profile Kiev-Gomel, *Geophys. J.,* **7**(2), 37–42.

Karpinsky, A.P., 1883. The remarks on the character of dislocations of rocks in the southern part of European Russia, *Min. J.,* **III,** 45–55 (in Russian).

Keller, G.R. & Baldridge, W.S., 1995. The Southern Oklahoma aulacogen, in Continental Rifts: Evolution, Structure, Tectonics, pp. 427–435, ed. Olsen, K.H., Elsevier.

Keller, G.R. & Stephenson, R.A., 2007. The Southern Oklahoma and Dnieper-Donets aulacogens: a comparative analysis, *Geol. Soc. Am. Mem.,* **200,** 1–17.

Khain, V.E., 1977. *Regional Geotectonics. Extra-Alpine Europe and Western Asia*, pp. 359, Nedra, (in Russian).

Kivshik, M.K., Stovba, S.M. & Turchanenko, M.T., 1993. Certain features of the Dnieper–Donets depression structure from the regional seismic-stratigraphic investigations data, *Geol. J.,* **2,** 87–98 (in Russian).

Kolomiyets, A.V. & Kharchenko, A.V., 2008. Tuning parallel computations for low-bandwidth network, *Comput. Math.,* **1,** 63–69 (in Russian).

Komminaho, K., 1998. *Software Manual for Programs MODEL and XRAYS: A Graphical Interface for SEIS83 Program Package,* Vol. 20, pp. 31, University of Oulu, Dep. of Geophys., Rep.

Koroleva, T.Yu., Yanovskaya, T.B. & Patrusheva, S.S., 2010. Velocity structure of the upper mantle of the East European platform according to seismic noise data, *Izv., Phys. Solid Earth,* **46**(10), 839–848.

Kostyukevich, A.S., Starostenko, V.I. & Stephenson, R.A., 2000. The full-wave images of the models of the deep lithosphere structures constructed according to DSS and CDP data interpretation, *Geophys. J.,* **22**(4), 96–98.

Kozlovskaya, E., Janik, T., Yliniemi, J., Karatayev, G. & Grad, M., 2004. Density-velocity relationship in the upper lithosphere obtained from *P*- and *S*-wave velocity models along the EUROBRIDGE'97 seismic profile and gravity data, *Acta Geophys. Pol.,* **52**(4), 1–28.

Kozlovskaya, E.G., Karatayev, G.I. & Yliniemi, J., 2001. Lithosphere structure along the northern part of EUROBRIDGE in Lithuania; results from integrated interpretation of DSS and gravity data, *Tectonophysics,* **339**(1–2), 177–191.

Kusznir, N.J., Stovba, S.M., Stephenson, R.A. & Poplavskii, K.N., 1996a. The formation of the northwestern Dnepr-Donets Basin: 2-D forward and reverse syn-rift and post-rift modelling, *Tectonophysics,* **268**(1–4), 237–255.

Kusznir, N.J., Kovkhuto, A. & Stephenson, R.A. 1996b. Syn-rift evolution of the Pripyat Trough: constraints from structural and stratigraphic modelling, *Tectonophysics,* **268**(1–4), 221–236.

Kutas, R.I. & Gordienko, V.V., 1971. *Heat Flow of Ukraine*, pp. 147, Naukova Dumka.

Lukin, A.Ye., 1997. *Lithogeodynamic Factors of Oil and Gas Accumulation in Aulacogenic Basins*, pp. 223, Naukova Dumka.

Lyashkevich, Z.M., 1987. *Magmatism of Pripyat-Dnieper-Donets paleorift*, pp 176, Naukova Dumka, (in Russian).

Lyashkevich, Z.M. & Marushkin, A.I., 1982. *Volcanic Formations of Dnieper-Donets Depression*, pp. 180, Naukova Dumka. (in Russian).

Lyngsie, S.B., Thybo, H. & Lang, R., 2007. Rifting and lower crustal reflectivity: a case study of the intracratonic Dniepr-Donets rift zone, Ukraine, *J. geophys. Res.,* **112**(B12), B12402, doi:10.1029/2006JB004795.

Makris, J. & Ginzburg, A., 1987. The Afar Depression: transition between continental rifting and sea-floor spreading, *Tectonophysics,* **141**(1–3), 199–214.

Markwick, A.J.W., Downes, H. & Veretennikov, N., 2001. The lower crust of SE Belarus: petrological, geophysical and geochemical constraints from xenoliths, *Tectonophysics,* **339**(1–2), 215–237.

Maystrenko, Y. *et al.*, 2003. Crustal-scale pop-up structure in cratonic lithosphere: DOBRE deep seismic reflection study of the Donbas fold belt, Ukraine, *Geology,* **31**(8), 733–736.

Nikishin, A.M., Ziegler, P.A. & Stephenson, R.A. *et al.* 1996. Late Precambrian to Triassic history of the East European Craton: dynamics of sedimentary basin evolution, *Tectonophysics,* **268**(1–4), 23–63.

Pashkevich, I.K., Orlyuk, M.I. & Lebed, T.V., 2014. Magnetic data, fault tectonics of consolidated Earth's crust and oil-and-gas content of the Dnieper-Donets aulacogen, *Geophys. J.,* **1**(36), 64–80 (in Russian).

Pavlenkova, N.I., 1995. Double Moho in the Dnieper-Donets basin, *C.R. Acad. Sci., Paris II,* **321,** 85–93.

Pobedash, M.S., 2015. Regional CDP seismic studies within the southern flank of the north-western part of the Dnieper-Donets Basin, Report TP 113/08 of DGP "Ukrgeofizika" Technology Center, Kiev.

Poplavskii, K.N., Podladchikov, Yu. & Stephenson, R.A., 2001. Two-dimensional inverse modeling of sedimentary basin subsidence, *J. geophys. Res.,* **106**(B4), 6657–6671.

Prodehl, C., Mueller, St., Glahn, A., Gutscher, M. & Haak, V., 1992. Lithospheric cross sections of the European Cenozoic rift system, *Tectonophysics,* **208**(1–3), 113–138.

Saintot, A., Stephenson, R., Brem, A., Stovba, S. & Privalov, V., 2003. Paleostress field reconstruction and revised tectonic history of the Donbas fold and thrust belt (Ukraine and Russia), *Tectonics,* **22**(5), 1059, doi:10.1029/2002TC001366.

Saintot, A., Stephenson, R.A., Stovba, S., Brunet, M.-F., Yegorova, T. & Starostenko, V., 2006. The evolution of the southern margin of Eastern Europe (Eastern European and Scythian platforms) from the latest Precambrian-Early Palaeozoic to the Early Cretaceous, in *European Lithosphere Dynamics, Memoirs,* Vol. 32, pp. 481–505, eds Gee, D.G. & Stephenson, R.A., Geological Society of London.

Shchipansky, A.A. & Bogdanova, S.V., 1996. The Sarmatian crustal segment: Precambrian correlation between the Voronezh Massif and the Ukrainian Shield across the Dniepr-Donets Aulacogen, *Tectonophysics,* **268,** 109–125,

Sollogub, V.B. (ed.), 1980. *The Structure of the Earth's Crust of the Central and Eastern Europe According to Geophysical Research Data*, pp. 280, Naukova Dumka (in Russian).

Sollogub, V.B., 1986. *Lithosphere of Ukraine*, pp. 154, Naukova Dumka (in Russian).

Sollogub, V.B., Borodulin, M.I. & Chekunov, A.V., 1977. Deep structure of Donbass and adjoining territories, *Geol. J.,* **37,** 23–31 (in Russian).

Środa, P. *et al.*, 2006. Crustal and upper mantle structure of the Western Carpathians from CELEBRATION 2000 profiles CEL01 and CEL04: Seismic models and geological implications, *Geophys. J. Int.,* **167,** 737–760 (doi:10.1111/j.1365-246X.2006.03104.x).

Starostenko, V. *et al.*, 2013a. Seismic velocity model of the crust and upper mantle along profile PANCAKE across the Carpathians between the Pannonian Basin and the East European Craton, *Tectonophysics,* **608,** 1049–1072.

Starostenko, V. *et al.*, 2013b. Mesozoic(?) lithosphere-scale buckling of the East European Craton in southern Ukraine: DOBRE-4 deep seismic profile, *J. geophys. Int.,* **195,** 740–766.

Starostenko, V.I. & Stephenson, R.I., 2006. Project GEORIFT: Deep structure and evolution of the Dnepr-Donets basin and Karpinsky Swell, in *Structure and Dynamics of the Lithosphere of Eastern Europe, Results of the Research on the EUROPROBE Program*, pp. 291–342, ed. Pavlenkova, N.I., GEOKART: GEOS (in Russian).

Starostenko, V.I., Kozlenko, V.G., Oganesyan, S.M., Shen, E.L., Oganesyan, M.G., Yegorova, T.P. & Dyadura, G.V., 1986. 3-D distribution of the density in the crust of the Dnieper Graben, *Geophys. J.,* **8,** 3–19 (in Russian).

Starostenko, V.I., Danilenko, V.A., Vengrovitch, D.B., Kutas, R.I., Stovba, S.M., Stephenson, R.A. & Kharitonov, O.M., 1999. A new geodynamical–thermal model of rift evolution, with application to the Dnieper–Donets Basin, Ukraine, *Tectonophysics,* **313,** 29–40.

Stephenson, R.A. (ed.), 2004. EUROPROBE GeoRift 3: intraplate tectonics and basin dynamics, *Tectonophysics,* **381,** 273.

Stephenson, R.A. & the EUROPROBE Intraplate Tectonics and Basin Dynamics Working Groups, 1993. Continental rift development in Precambrian and Phanerozoic Europe: EUROPROBE and the Dnieper-Donets rift and Polish Trough basins, *Sedimentary Geol.,* **86,** 159–175.

Stephenson, R.A., Wilson, M., de Boorder, H. & Starostenko, V.I. (eds), 1996. EUROPROBE: Intraplate tectonics and basin dynamics of the Eastern European platform preface, *Tectonophysics,* **268,** vii–x.

Stephenson, R.A., Wilson, M. & Starostenko, V.I. (eds), 1999. EUROPROBE GeoRift, volume 2: Intraplate Tectonics and Basin Dynamics of the Eastern European Craton and Its Margins, *Tectonophysics,* **313**, VII–IX.

Stephenson, R.A., Stovba, S.M. & Starostenko, V.I., 2001. Pripyat–Dnieper–Donets Basin: implications for dynamics of rifting and the tectonic history of northern Peri-Tethyan Platform, in *Peri-Tethys Memoir 6: Peri-Tethyan Rift/Wrench Basins and Passive Margins*, vol. **186**, pp. 369–406, eds Ziegler, P.A., Cavazza, W., Robertson, A.H.F. & Crasquin-Soleau, S., Mémoires du Muséum National d'Histoire Naturelle.

Stephenson, R.A., Yegorova, T.P., Brunet, M.-F., Stovba, S., Wilson, M., Starostenko, V., Saintot, A. & Kusznir, N., 2006. Late Palaeozoic intra- and pericratonic basins on the East European Craton and its margins, in *European Lithosphere Dynamics, Memoirs,* Vol. 32, pp. 463–479, eds. Gee, D.G. & Stephenson, R.A, Geological Society of London.

Stovba, S.M. & Stephenson, R.A., 1999. The Donbas Foldbelt: its relationships with the uninverted Donets segment of the Dniepr–Donets Basin, Ukraine, *Tectonophysics,* **313,** 59–83.

Stovba, S., Stephenson, R. & Dvorianin, E., 1995. Dnieper-Donets Basin, Ukraine, main observations from regional seismic reflection profiles, *C.R. Acad. Sci., Paris II,* **321,** 1103–1110.

Stovba, S.M., Stephenson, R.A. & Kivshik, M., 1996. Structural features and evolution of the Dniepr-Donets Basin, Ukraine, from regional seismic reflection profiles, *Tectonophysics,* **268,** 127–147.

Thybo, H., Maguire, P.K.H., Birt, C. & Perchuć, E., 2000. Seismic reflectivity and magmatic underplating beneath the Kenya Rift, *Geophys. Res. Lett.,* **27,** 2745–2748.

Thybo, H. *et al.*, 2003. Upper lithospheric seismic velocity structure across the Pripyat Trough and the Ukrainian Shield along the EUROBRIDGE'97 profile, *Tectonophysics,* **371,** 41–79.

Ulmishek, G.F., Bogino, V.A., Keller, M.B. & Poznyakevich, Z.L., 1994. Structure, stratigraphy and petroleum geology of the Pripyat and Dniepr–Donets basins, in *Byelarus and Ukraine Interior Rift Basins*, vol. **59**, pp. 125–156, ed. Landon, S. M., American Association of Petroleum Geologists, Memoirs.

Van Wees, J.D., Stephenson, R.A., Stovba, S.M. & Shymanovskyi, V. A., 1996. Tectonic variation in the Dniepr-Donets Basin from automated modelling of backstripped subsidence curves, *Tectonophysics,* **268,** 257–280.

Wilson, M., 1993. Magmatism and the geodynamics of basin formation, *Sedimentary Geol.,* **86,** 5–29.

Wilson, M. & Lyashkevich, Z.M., 1996. Magmatism and the geodynamics of rifting of the Pripyat-Dnieper-Donets rift, East European Platform, *Tectonophysics,* **268,** 65–81.

Yegorova, T., Bakhmutov, V., Janik, T. & Grad, M., 2011. Joint geophysical and petrological models for the lithosphere structure of the Antarctic Peninsula continental margin, *Geophys. J. Int.,* **184,** 90–110.

Yegorova, T.P., Stephenson, R.A., Kozlenko, V.G., Starostenko, V.I. & Legostaeva, O.V., 1999. 3-D gravity analysis of the Dniepr–Donets Basin and Donbas Foldbelt, Ukraine, *Tectonophysics,* **313,** 41–58.

Yegorova, T.P., Stephenson, R.A., Kostyuchenko, S.L., Baranova, E.P., Starostenko, V.I. & Popolitov, K. E., 2004a. Structure of the lithosphere below the southern margin of the East European Craton (Ukraine and Russia) from gravity and seismic data, *Tectonophysics,* **381,** 81–100.

Yegorova, T.P., Starostenko, V.I., Kozlenko, V.G. & Yliniemi, J., 2004b. Lithosphere structure of the Ukrainian Shield and Pripyat Trough in the region of EUROBRIDGE-97 (Ukraine and Belarus) from gravity modelling, *Tectonophysics,* **381,** 29–59.

Zelt, C.A., 1994. *Software Package ZPLOT,* Bullard Laboratories, University of Cambridge.

Zonenshain, L.P., Kuzmin, M.I. & Natapov, L.M., 1990. *Geology of the USSR: A Plate-Tectonic Synthesis,* American Geophysical Union, Geodynamic Series, 21.